International Reviews in Physical Chemistry

ISSN: 0144-235X (Print) 1366-591X (Online) Journal homepage: http://www.tandfonline.com/loi/trpc20

The interaction of negative charge with carbon dioxide – insight into solvation, speciation and reductive activation from cluster studies

J. Mathias Weber

To cite this article: J. Mathias Weber (2014) The interaction of negative charge with carbon dioxide – insight into solvation, speciation and reductive activation from cluster studies, International Reviews in Physical Chemistry, 33:4, 489-519, DOI: 10.1080/0144235X.2014.969554

To link to this article: http://dx.doi.org/10.1080/0144235X.2014.969554

Published online: 06 Nov 2014.

Submit your article to this journal

Article views: 236

View related articles

View Crossmark data

Citing articles: 17 View citing articles

Full Terms & Conditions of access and use can be found at
http://www.tandfonline.com/action/journalInformation?journalCode=trpc20

Download by: [Universitaetsbibliothek Innsbruck] **Date:** 31 May 2017, At: 04:43

International Reviews in Physical Chemistry, 2014
Vol. 33, No. 4, 489–519, http://dx.doi.org/10.1080/0144235X.2014.969554

Taylor & Francis
Taylor & Francis Group

The interaction of negative charge with carbon dioxide – insight into solvation, speciation and reductive activation from cluster studies

J. Mathias Weber*

JILA and Department of Chemistry and Biochemistry, University of Colorado, Boulder, CO 80309, USA

(*Received 4 September 2014; final version received 23 September 2014*)

The interaction of CO_2 with negative charge is of high importance in many natural and industrial processes, since reductive activation is one of the most common and convenient ways to chemically unlock this robust molecule. While free CO_2 does not form stable anions, the accessibility of low-lying molecular orbitals is critical for its chemical versatility and allows CO_2 to act as solvent as well as a reaction partner for negative ions. Experiments on mass selected cluster ions are highly suitable for the study of the fundamental properties of CO_2 and its interaction with excess electrons and anions, since they circumvent many problems associated with experiments in the condensed phase. The combination of mass spectrometry, laser spectroscopy and quantum chemical calculations results in a powerful tool set to address questions of reactivity, ion speciation and solvation, and they can provide key information to understanding the ion chemistry of CO_2.

Keywords: clusters; speciation; solvation; reduction; C–O activation; catalysis

Contents

*Email: weberjm@jila.colorado.edu

© 2014 Taylor & Francis

1. Introduction

Carbon dioxide is an important product of metabolic and combustion processes and an essential ingredient for all plant life. The relative inertness of CO_2 has made it attractive for use in food industry, as a refrigerant, and as a 'green' organic solvent in the form of supercritical CO_2. However, its increasing concentration in Earth's atmosphere together with its impact as a greenhouse gas and as an ocean acidifier renders it a pollutant, and it is of great interest to reduce the global output of CO_2 from industrial processes as well as from fuel combustion. Carbon dioxide sequestration by chemical means may be one way to reduce the atmospheric CO_2 content. However, CO_2 could be a great renewable source of carbon, and it would very interesting to use CO_2 as feedstock to convert into chemical fuels to help create a carbon-neutral fuel cycle.

As a result of its enormous importance, the chemistry and physics of CO_2 are of great interest. Its interaction with negative charge is particularly relevant, since the most convenient access to its chemistry is through reduction. While free CO_2 molecules do not form long-lived negative ions, CO_2 can incorporate negative charge into low-lying molecular orbitals, and the resulting negative ion states can be metastable or they can be stabilised by solvation. This leads to a high chemical versatility, and it opens an important pathway to the industrial use of CO_2 as a chemical feedstock through reductive activation [1–11].

The interaction of ions with their chemical environment plays an important role in many areas of chemistry, from atmospheric chemistry and astrochemistry to electrochemistry, catalysis and biochemistry [12–25]. For example, solvation has an important mediating role in chemistry, e.g. by stabilising ions, enabling ion transport or allowing reaction partners to encounter each other in solutions. More importantly, solvent–solute interaction can change the properties of both ionic solute and neutral solvent in profound ways that significantly impact their chemical behaviour. Therefore, an in-depth, molecular-level understanding of many ionic chemical processes requires a fundamental understanding of the physical aspects of ion–molecule interactions and ion solvation.

For several reasons, studying such interactions in a condensed phase environment is very difficult. Fluctuations in the solvent shell around the ion and the presence of solvent molecules distant from the ions under study can mask or complicate the response of the species of interest. Moreover, speciation in solutions can be problematic, as reactions with solvent molecules or ligand exchange reactions can result in solutions of essentially unknown composition, and the solute ion of interest may even be a transient species. Solid interfaces present their own challenges, especially if the interface of interest is not a single crystal facet, but structurally more heterogeneous, as is the case with many catalysts [10,26,27]. Many applications, particularly in the field of heterogeneous electrocatalysis, combine the hardships of liquids and solids. As a result, our knowledge about the molecular-level details of CO_2 reduction is sparse.

Ion–molecule complexes and cluster ions *in vacuo* present a convenient way to circumvent many of these problems. Their key advantage is that they can be prepared by mass spectrometry, which allows precise control over the composition of these target systems. The behaviour of binary ion–molecule complexes can be studied to learn about pairwise interactions. Moreover, the chemical environment in the vicinity of an ion can be built and studied one molecule at a time in cluster ions. Analysis of the

properties of these ionic systems as a function of cluster size allows investigation of the molecular level details of the microsolvation environment of ions.

Mass selected ion–molecule complexes and clusters can be interrogated by a number of sensitive techniques. Mass spectrometry can reveal the reactivity of ions and determine ionic reaction products. Photoelectron spectroscopy of mass-selected anions can give insight into the electronic structure of both the anions and the neutral species remaining behind after electron emission. Photodissociation spectroscopy in the UV and visible spectral regions can probe the photophysics of ions and their behaviour in electronic excited states. Infrared photodissociation spectra encode effects of inter- and intramolecular forces and allow accessing structural information about the system under study. Of course, none of these techniques can reach their full interpretative potential without the powerful tools of quantum chemistry. In the past 20 years, great progress in method development has been made, and the accessibility of computational methods and the enormous increase in available computing power have been invaluable for the successes of cluster science. In turn, cluster ions are nearly perfect systems to push the envelope of quantum chemistry, since they represent a clean experimental approach to ever growing, but well-defined system size and increasing complexity.

In the present paper, we review work on anion–molecule complexes and cluster anions involving CO_2. Here, CO_2 can play the role as a solvent, but also as a charge carrier in the form of CO_2^- or related species. We will first describe the electronic and vibrational properties of CO_2 and CO_2^- in Section 2, followed by a discussion of the behaviour of neat CO_2 clusters with an excess negative charge in Section 3. In Section 4 we describe the interaction of CO_2 with a number of nonmetallic atomic and molecular anions, with its roles varying from a solvent to a reaction partner. We focus on anionic complexes of CO_2 with metal atoms in Section 5. Finally, we present an outlook towards future work in this area.

2. Properties and electronic structure of the CO_2^- anion

Neutral CO_2 is a linear molecule with $D_{\infty h}$ symmetry and a $^1\Sigma_g^+$ ground state. Its electronic structure can be visualised using a Walsh diagram [28] as shown in Figure 1. In the neutral molecule, the highest occupied molecular orbital (HOMO) is the $1\pi_g$ orbtial, which is fully occupied. Adding an excess electron into the lowest unoccupied molecular orbital (LUMO) of neutral CO_2 results in the population of the antibonding $2\pi_u$ orbital. As a result, the C–O distance in the anion (124 pm [29]) is longer than that in the neutral (116.1 pm [30]). In addition, the presence of the excess electron leads to a deformation of the molecule from the linear geometry of the neutral to a bent anion (C_{2v} symmetry). The bond angle has been determined by a variety of experimental [31–34] and theoretical [29,35] methods to be ca. 134°. In a linear geometry, the CO_2^- ion is in a $^2\Pi_u$ state, whose degeneracy is lifted upon deformation and splits into the $^2A_1$ ground state of the anion (with the excess electron in the $6a_1$ orbital) and a $^2B_1$ excited state (with the excess electron in the $2b_1$ orbital).

Most experiments on and nearly all spectroscopy of the CO_2^- anion have been performed in alkali halide [31,32] and rare gas [33,34,36–39] matrices, not on isolated CO_2^-, a fact that is a consequence of the instability of the bare anion. The vertical detachment energy (VDE) of CO_2^- has been measured by Bowen and coworkers to be ca. 1.4 eV [40] and calculated by Bartlett and coworkers to be ca. 1 eV [35]. However, Compton *et al.* determined the anion ground state to be (0.6 ± 0.2) eV *above* that of the neutral molecule, using electron transfer reactions in collisions with alkali atoms

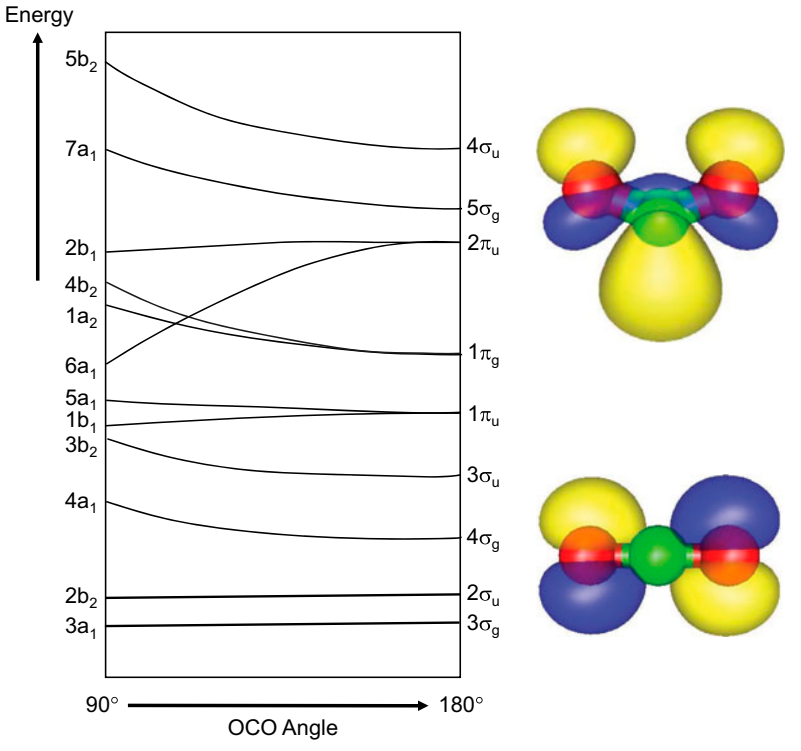

Figure 1. (Colour online) Left: Walsh diagram (schematically constructed after [28]) for CO_2, showing the molecular valence orbitals as a function of the OCO bond angle. For the symmetry notations in the bent geometry, we assume that the molecule is in the yz plane. Right: Structures and HOMOs of CO_2 (lower) and CO_2^- (upper), obtained from simple HF-SCF calculations. Note that only one of the degenerate π_g orbitals for the HOMO of the neutral molecule is shown. Colour scheme: green: C; red: O; blue/yellow: positive and negative signs of the orbital.

[41]. Quantum chemical calculations by Bartlett and coworkers [35] as well as by Cederbaum and coworkers [29] come to similar conclusions. In other words, the adiabatic electron affinity (AEA) of CO_2 is negative. The ground state of the anion is separated from the vibrationally excited electronic ground state of neutral CO_2 by a small barrier, typically calculated to be ca. 0.3 eV [35,42–45], although some of the highest level *ab initio* results by Sommerfeld and Cederbaum give an even lower barrier [29,46] (see Figure 2). As a result, the bare anion is thermodynamically unstable, and it can easily decay under electron emission by vibrational excitation and crossing of or tunnelling through the barrier. Consequently, CO_2^- ions have been observed only as metastable species with lifetimes ranging from tens of μs to ms. Bare CO_2^- ions have been produced in electron collisions with organic molecules [47] or CO_2 clusters [48], as well as in double electron transfer to CO_2^+ [49,50] and sputtering experiments [51]. However, with the exception of Bowen's photoelectron spectroscopy study [40], no spectroscopic data on bare ions exist beyond mass spectrometry, owing to their lifetime, which renders experiments on mass-selected CO_2^- ions difficult at best. While the isolated CO_2^- ion is metastable, it can be stabilised by solvation in matrices as well as a number of other environments (e.g. in clusters, see later Sections).

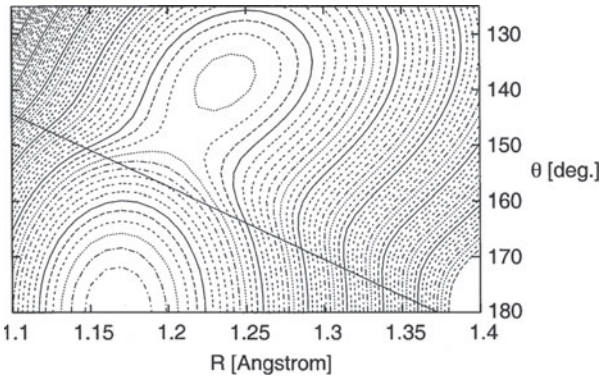

Figure 2. Contour plot of the CO_2/CO_2^- potential energy surface as a function of the CO bond length R (in Å) and the bond angle θ (in degrees). The energy origin is the minimum of neutral CO_2, and the energy difference between two contour lines is 0.05 eV. Reproduced from [29] with permission of The Royal Society of Chemistry.

Collisions of free electrons with isolated neutral CO_2 molecules only lead to transient negative ions (i.e. scattering resonances) with ultrashort lifetimes, which are formed by a $^2\Sigma_g^+$ virtual state at low collision energies (below 1 eV) and a $^2\Pi_u$ shape resonance at ca. 3.7 eV [52–64]. The former is due to vibrational excitation of the symmetric stretching mode, while the latter is caused by short-term capture into the LUMO of neutral CO_2. At higher energies, additional resonances appear, which have been proposed to be due to core-excited resonances [65,66]. The only stable electron attachment products for electron collsions with CO_2 are O^- ions [48,67]. We will not discuss electron scattering at isolated neutral CO_2 molecules further at this point, but rather revisit electron attachment to CO_2 clusters in Section 3.1.

Much of this review will concern the study of the interaction of CO_2 with negative charge by vibrational spectroscopy, so it is useful to discuss the vibrational properties of CO_2 and its anion. The three vibrational modes of neutral CO_2 are the symmetric C–O stretching vibration $\nu_1(\sigma_g^+)$, the doubly degenerate bending mode $\nu_2(\pi_u)$, and the antisymmetric C–O stretching vibration $\nu_3(\sigma_u^+)$. The antisymmetric stretching mode ν_3 is observed at 2349 cm^{-1} [68]. The fundamental transition of the bending mode ν_2 is observed at 667 cm^{-1} [68], making its overtone $2\nu_2$ nearly degenerate with the fundamental of the symmetric stretching mode ν_1 (at ca. 1333 cm^{-1}). This (accidental) degeneracy gives rise to one of the best-known examples of a Fermi resonance, with signatures observed at 1388.15 cm^{-1} and 1285.4 cm^{-1} [68]. This Fermi resonance of the states $(\nu_1\nu_2\nu_3) = (0\,2\,0)$ and $(1\,0\,0)$ has a corresponding Fermi dyad around 3650 cm^{-1}, formed by the respective combination bands with one quantum of ν_3, $[(0\,2\,1)\|(1\,0\,1)]$. Several other Fermi resonances are also in existence, for example the Fermi dyad $[(0\,3\,0)\|(1\,2\,0)]$ around 2000 cm^{-1}.

The vibrational energies in CO_2^- are red-shifted from their corresponding counterparts in neutral CO_2, since the presence of the excess electron in an antibonding orbital weakens the C–O bonds. As we will see in Section 5, the antisymmetric stretching mode ν_3 can serve as a probe for the excess charge density on a CO_2 molecule or on an OCO functional group. Infrared vibrational spectroscopy of CO_2^- has been performed in rare gas matrices, notably by Thompson and Jacox [34] and by Zhou and Andrews [33]. The most accurate data of the intrinsic spectroscopic properties of CO_2^-

come from these experiments, but we note that the direction and magnitude of matrix-induced shifts are not known and can amount to tens of cm^{-1}. The most intense fundamental transition is the antisymmetric C–O stretching mode $\nu_3(b_2)$, measured at 1658.3 cm^{-1} in Ne [34] and at 1657.0 cm^{-1} in Ar [33]. In alkali halide matrices, the ν_3 mode was observed to be shifted by ca. 10–20 cm^{-1} to higher wavenumbers [32]. The symmetric C–O stretching mode $\nu_1(a_1)$ and the bending mode $\nu_2(a_1)$ were measured in a Ne matrix at 1253.8 cm^{-1} and at 714.1 cm^{-1}, respectively [34]. The change in the vibrational energies upon forming a CO_2^- ion lifts the degeneracy of the bending mode overtone and the symmetric stretching mode, thereby weakening their coupling and – for all practical purposes – destroying the prototypical Fermi resonance of these vibrational levels observed in the neutral molecule.

The electronic spectrum of CO_2^- is not well explored. A γ-irradiated crystalline matrix of NaCOOH shows three absorption bands attributed to CO_2^- with maxima at ca. 3.65, 4.43 and 4.96 eV [69]. In contrast, only a single band at around 3.40 eV was observed in similar experiments in alkali halide matrices [32], and spectra in aqueous solution only exhibit a single peak at ca. 4.96 eV [70] assigned to CO_2^- . The band at 3.65 eV has been previously assigned to the $^2A_1 \rightarrow {}^2B_1$ transition [32,69], and we will revisit this transition in Section 4.3.

The CO_2^- anion in the absence of a stabilising environment remains an elusive species, and while the electron scattering behaviour is well established, the properties of the anion in its ground state deserve continued attention. As we will see throughout this review, the properties of CO_2^- give rise to rich chemistry and physics in cluster environments, and we can hope to learn much about the bulk behaviour of CO_2^- through understanding them.

3. Neat $(CO_2)_n^-$ clusters

3.1. *Electron attachment to neutral CO_2 clusters*

Electron attachment to neutral $(CO_2)_N$ clusters generated in supersonic expansions has been the method of choice to generate neat $(CO_2)_n^-$ cluster ions. In the simplest case, this involves injection of electrons into the high-density region of a supersonic expansion of neat CO_2 or of a suitable carrier gas (e.g. rage gases) seeded with CO_2. Collisions of slow electrons with energies up to a few eV can lead to the formation of negative ions. These slow electrons are either primary electrons injected into the expansion or secondary electrons from an electron impact plasma. The latter process has been widely employed in a type of ion source which goes back to work by Lineberger and coworkers [71]. This ion source type has been used extensively to study the properties of mass-selected cluster anions in general, and many of the experiments discussed in this review are based on it. However, since there is no control over the kinetic energy of the secondary electrons that ultimately lead to anion formation, only limited information on the actual attachment process can be obtained this way.

Electron attachment to neutral CO_2 clusters is of interest not only for gas phase studies, but can also yield deeper insight into the fundamental processes during electron injection into, electron transport in and electron transfer between species in supercritical CO_2 (see, e.g. [72,73]), which has become more and more a focal point for 'green' chemistry techniques. In addition, the chemistry of CO_2 in astrochemical [74,75] and atmospheric [76] contexts may be impacted by such processes.

The interaction of neutral $(CO_2)_N$ clusters with energy-selected free electrons has been used to study the formation of $(CO_2)_n^-$ cluster ions ($n \leq N$) in more detail, notably

by the groups of Hotop and of Märk. Electron attachment to CO_2 clusters occurs via evaporation of neutral CO_2 molecules along the reaction sequence

$$(CO_2)_N + e^- \rightarrow (CO_2)_N^{-*} \rightarrow (CO_2)_n^- + (N-n)CO_2. \quad (1)$$

Several broad structures are visible in the anion formation cross section of neat $(CO_2)_n^-$ clusters (see Figure 3). At low energies, and at electron energy resolutions around 0.1 eV or broader, a 'zero-eV' resonance is observed [48,66,77–79]. At electron energies above 1 eV, broad resonances at ca. 3, 8 and 12 eV are found. The resonance at 3 eV has been attributed to the cluster analogue of the $^2\Pi_u$ shape resonance in isolated CO_2 molecules [48,65,66]. Different from scattering at isolated molecules, the cluster environment allows redistribution of the electron energy into vibrational degrees of freedom of the cluster and subsequent evaporation of CO_2 monomer units. This energy dissipation process facilitates the formation of $(CO_2)_n^-$ ions. At energies slightly above the peak of the $^2\Pi_u$ shape resonance, dissociative attachment resulting in $[O(CO_2)_n]^-$ clusters becomes energetically allowed, where the initial capture still proceeds via the $^2\Pi_u$ resonance [48,65,66]. The features at higher energies have been attributed to core-excited resonances [65,66].

At very high resolution, it becomes clear that the 'zero-eV' feature is in fact composed of several resonances (see Figure 4) that show a strong cluster size dependence [80,81]. These features can be traced to vibrational Feshbach resonances (VFRs). Such resonances are states where the excess electron is trapped in the field of a vibrationally excited molecular or cluster 'host' [82–86]. In the case of CO_2 clusters, VFRs corresponding to the excitated vibrational state (0 1 0) as well as the Fermi polyads [(0 2 0)||(1 0 0)], [(0 3 0)||(1 1 0)] and [(0 4 0)||(1 2 0)||(2 0 0)] have been observed [80,81]. These VFRs shift to lower energies with increasing cluster size by ca. 12 meV per CO_2 unit. Fabrikant used *R*-matrix calculations to describe these VFRs [80,81,87–91], modelling the electron–cluster interaction by the interaction with the cluster size dependent polarisability $\alpha(N)$ outside the cluster, and a constant potential $U_0(N)$ inside the cluster (radius R_N):

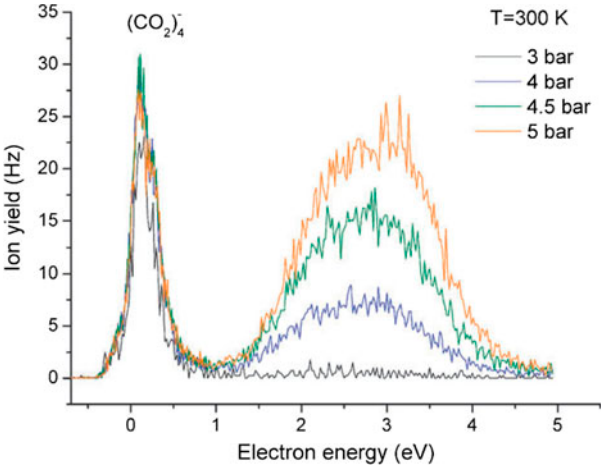

Figure 3. (Colour online) Ion formation yield of $(CO_2)_4^-$ as a function of electron kinetic energy at ca. 0.1 eV energy resolution. The relative intensities of the higher energy features increase with increasing stagnation pressure, indicating that relatively large neutral parent clusters are needed, so several CO_2 units can be evaporated in order to dissipate the energy deposited into the parent cluster upon attachment. Reproduced from [66] with permission of The Royal Society of Chemistry.

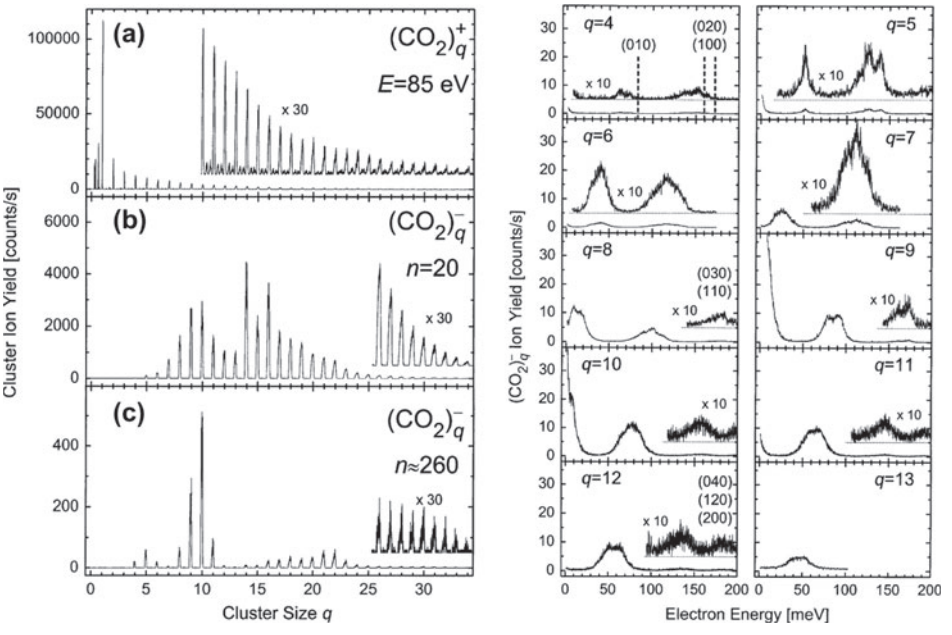

Figure 4. Left: Mass spectra of $(CO_2)_q^{\pm}$ cluster ions resulting from electron impact ionisation (a) and RET (b and c). Note that the principal quantum numbers n^* are denoted n in this figure. (a) Mass spectrum of positive cluster ions due to 85 eV electron impact. (b) Mass spectrum of cluster anions due to RET involving $K^{**}(20d)$ atoms ($E = 35$ meV). (c) Mass spectrum of cluster anions resulting from threshold electron attachment involving K^{**} Rydberg atoms with a band of principal quantum numbers around 260 ($E \approx 0.2$ meV). Right: VFRs in the formation yield of $(CO_2)_q^-$ ions [80,81]. Reprinted from [81] with permission from Elsevier.

$$V_N(r) = \begin{cases} U_0 & \text{if } r < R_N \\ -\frac{Ne^2\alpha(N)}{2r^4} & \text{otherwise} \end{cases} \tag{2}$$

The red-shift of the VFRs is mainly governed by the size-dependent polarisability term. The behaviour close to the 0 eV threshold varies strongly with cluster size, depending on whether one of the VFRs is located in the immediate vicinity of the zero-eV threshold.

Another strategy to study the formation of $(CO_2)_n^-$ clusters is the transfer of Ryd-berg electrons from highly excited atoms to neutral $(CO_2)_N$ clusters. Such experiments were first performed without state selective excitation of the atomic collision partner in experiments by Kondow and coworkers [92,93]. Hotop and coworkers later performed experiments using state-selected Ar and K Rydberg atoms [80,81,94,95]. For all approaches (free as well as Rydberg electrons) used to generate $(CO_2)_n^-$ cluster ions, the ion abundance varies strongly with cluster size [65,80,81,93–95], with 'magic numbers' at $n = 5, 10, 14, 16$ as well as at several larger sizes [96]. This is maybe most strongly observable in Rydberg electron transfer (RET), where the appearance of local ion abundance maxima is also strongly dependent on the principal quantum number n^*(see Figure 4). In RET, the ion yield is proportional to the rate coefficient $k(n^*, l)$, which depends on the velocity distribution $f_v(n^*, l)$ via

$$k(n^*, l) = \int_0^\infty \sigma(v) \cdot v \cdot f_v(n^*, l) \mathrm{d}v, \tag{3}$$

where σ is the electron attachment cross section, v the electron velocity, and l the angular momentum quantum number. At high principal quantum numbers, $f_v(n^*, l)$ samples mostly very low velocities, consequently emphasising the electron attachment cross sections at very low kinetic energies. In contrast, the velocity distribution function at lower principal quantum numbers includes contributions from higher velocities. As a result, the RET mass spectrum at very high principal quantum numbers reflects only the immediate threshold region of the attachment cross section. The VFR positions in CO_2 clusters are strongly size dependent and govern the electron attachment cross section close to threshold. Consequently, they determine which *neutral* parent clusters $(CO_2)_N$ can attach an electron efficiently, particularly for RET. The abundance of the resulting $(CO_2)_n^-$ cluster *anions*, however, is also influenced by the survival probability of the nascent ions, which depends on the energy deposited in the cluster upon electron attachment. The widths of the VFRs suggest that the fragment ions are mostly the products of attachment to a single cluster size [80,81], at least for electron attachment close to threshold. At larger collision energies, the clusters with $n = 10$, 14 and 16 are more abundant than others, pointing to a higher stability of these cluster sizes with respect to monomer evaporation [97].

As we have seen, electron attachment to CO_2 clusters shows a plethora of interesting chemical and physical processes. We will now turn to the properties of the CO_2 clusters formed in such processes.

3.2. *Structural and electronic properties of neat $(CO_2)_n^-$ cluster ions*

The central question regarding the properties of $(CO_2)_n^-$ cluster ions is how they accommodate the excess negative charge. Since the CO_2^- ion is metastable, one could in principle expect that the charge is distributed over all CO_2 molecules in the cluster. Water clusters constitute an example of this case, where the excess electron is bound to the electrostatic field created by the water molecules, but is not associated with the valence orbitals of any single water molecule. Alternatively, the charge carrying species could be generated by a subset of the CO_2 molecules in the cluster, or even a single CO_2 molecule, if the CO_2^- monomer ion could be sufficiently stabilised by solvation.

Let us first discuss the properties of the smallest 'cluster' anion, the dimer. Early *ab initio* work at Hartree–Fock (HF) [102,103] and post-HF levels by Jordan and coworkers [98] identified two structural motifs for $(CO_2)_2^-$ (see Figure 5). In the 'monomer anion' motif, the charge is mostly localised on a single CO_2 molecule, while

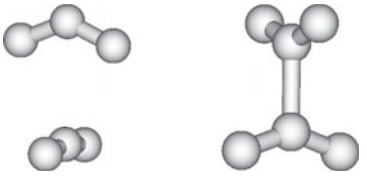

Figure 5. The 'monomer' (left) and 'dimer' (right) structural motifs for the $(CO_2)_2^-$ anion. Note that there are additional conformers of the 'monomer' motif with C_s symmetry [98–100]. Reprinted with permission from [101]. Copyright (2003), AIP Publishing LLC.

the second CO_2 plays the role of a solvent. In the 'dimer anion' motif, the charge is symmetrically distributed over both CO_2 moieties, and a C–C bond is formed between the two, reminiscent of the structure of the oxalate dianion. Later work by Nagata and coworkers at the MP2 level [99,100] extended these studies to larger clusters, up to $n = 6$. The most recent and highest level investigation was performed by Sommerfeld and Posset [101] at various coupled-cluster levels up to $n = 5$. The two different structural forms are energetically close, but for the small cluster sizes studied in the theoretical work cited above, the D_{2d} dimer anion motif is lower than the monomer motif. Both motifs have been recovered in matrix isolation work [33,34], and the dimer motif has been found to be the dominant structure. The photoelectron spectrum of $(CO_2)_2^-$ has been studied experimentally by several groups, including those of Johnson, Bowen, Nagata and Sanov. It shows a broad, unstructured peak at 2.79(2) eV [104] with an unresolved vibrational progression [40,104–106]. The peak of the photoelectron spectrum encodes the VDE of the ion, and the AEA is estimated to be ca. 1 eV lower.

Similar to the case of $(CO_2)_2^-$ dimer anion, photoelectron spectra of $(CO_2)_n^-$ cluster ions show only broad features [104–106], which point to large geometry differences between the anionic and neutral species involved. The groups of Johnson and of Nagata found that the VDEs of CO_2 cluster anions show pronounced discontinuities [104,105] at cluster sizes $n = 6$ and 14 (see Figure 6). The infrared spectra of $(CO_2)_n^-$ cluster ions reported jointly by the Johnson and Weber groups show similarly abrupt changes for the same cluster sizes [107], although the changes around $n = 6$ are more gradual (see Figure 6). These two independent observations show unambiguously that the charge carrying species changes as a function of cluster size, and they allow us to draw structural conclusions on the nature of the core ions as well. As mentioned above, the CO_2^- ion is only metastable, while the $(CO_2)_2^-$ dimer anion is likely to be a stable species. This suggests that the small clusters consist of dimer anions that are solvated by additional CO_2 monomer units. The infrared spectra of $(CO_2)_n^-$ cluster ions are dominated by strong peaks at wavenumbers slightly lower than 2349 cm^{-1} . This peak

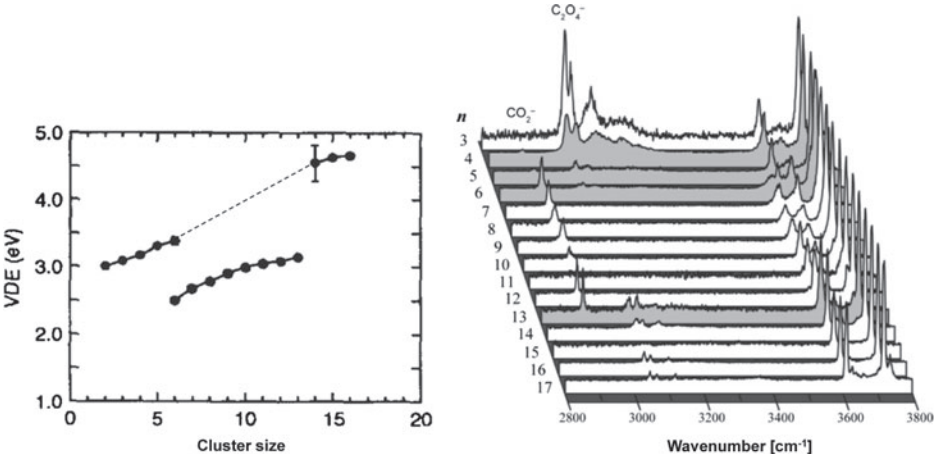

Figure 6. Size evolution of the vertical detachment energies (left, adapted from [105] with permission from Elsevier) and vibrational spectra (right, reprinted with permission from [107], copyright (2005) American Chemical Society) for $(CO_2)_n^-$ anions. The dashed line is meant to guide the eye.

is assigned to the antisymmetric stretching vibration of a neutral CO_2 molecule that is only weakly perturbed by its chemical environment and plays the role of a solvent. The [(0 2 1)||(1 0 1)] Fermi resonance is also present in these spectra with peaks around 3600 cm^{-1} and 3720 cm^{-1}, which are also signatures of solvent CO_2 molecules.

In addition to these solvent signatures, the spectra of the small clusters ($n = 3$–6) show a set of peaks between 3000 and 3200 cm^{-1} that have been identified as signatures of the D_{2d} form of the $(CO_2)_2^-$ dimer anion [33,107]. Here, the most intense, lowest energy peak is assigned to the combination band of the $\nu_5(b_2)$ and the $\nu_7(e)$ stretching fundamentals of the dimer, which are the out-of-phase motions of the symmetric and antisymmetric stretching modes of the two CO_2 moieties [107]. The peak is accompanied by an unidentified shoulder and a band about 76 cm^{-1} to the blue, which has been assigned to the $\nu_5 + \nu_7 + \nu_4$ combination band, where ν_4 is the C–C torsional mode. The assignment of the bands in the 3000–3200 cm^{-1} region corroborates the identification of the dimer anion as the core species in the small cluster regime ($n = 3$–6) which was made based on photoelectron data [104,105].

In the size region $n = 6$–13, the signature of the dimer anion vanishes and is replaced by peaks at ca. 2920 and 3640 cm^{-1} [107], concomitant with the lowering of the VDE by ca. 1 eV and a decrease in the overall width of the photoelectron bands [104,105], heralding a change in the nature of the charge carrier. The infrared bands shown in Figure 6 in this size regime can be identified as the (1 0 1) and (1 1 1) combination bands of a CO_2^- ion, based on matrix isolation spectroscopy [34]. This means that the charge carrying species is a CO_2^- monomer anion in this size range. The cause for this core-switching behaviour is the balance between the electronic stability of the charge carrier and solvation energy. Electronic stability is favouring the dimer core structure. In contrast, following the Born model for ion solvation [108], the solvation energy term lowers the energy of the monomer core more than that of the dimer, since $\Delta G_{solv} \propto 1/R_i$, and solvation of a more compact charge distribution (radius R_i) results in a higher solvation energy gain ΔG_{solv}. At $n = 6$, this balance tips in favour of a solvated monomer anion as the charge carrier [107]. Interestingly, angular distributions measured in photoelectron imaging experiments [109] show strong similarities regardless whether the charge carrier is CO_2^- or $C_2O_4^-$. The origin of this similarity is the fact that the HOMO of $C_2O_4^-$ can be treated as a linear combination of two monomer units.

As mentioned above, there is a second discontinuity at $n \geq 14$, where the infrared spectra revert to the dimer signature (with a vanishing monomer signature) and the VDE jumps back to higher values, continuing the trend of the small cluster size region (see Figure 6). This second core ion switch is caused by filling the first solvation shell of CO_2^- at $n = 13$ [107]. A solvent molecule added to a cluster with a full first solvation shell will have only little interaction with the charge carrier, and therefore the gain of solvation energy will be very small. At this point, it is more favourable to delocalise the charge and restore the dimer anion as a charge carrier, since it is larger and will therefore accommodate more solvent molecules in its first solvation shell. This observation is particularly interesting, since it highlights the effects of the molecular nature of solvation, which in this case overcomes simple dielectric effects. We note that the identity of the charge carriers in all three size regimes has recently been corroborated in the region of fundamental transitions as well [110–112].

The binding energies of solvent CO_2 molecules in $(CO_2)_n^-$ ions are strongly dependent on cluster size. At small cluster sizes ($n \leq 14$), they can be roughly estimated to be around 0.35–0.4 eV, based on the number of CO_2 units lost from clusters in this size upon infrared excitation [107,110,111], assuming that the internal energy of the cluster

is based on the theory of an evaporative ensemble [113]. It is to be expected that the binding energy varies non-monotonically with cluster size for small clusters, as the magic numbers in the formation efficiency are tied to cluster stability (see above). In larger clusters, the average binding energy of solvent CO_2 molecules has been experimentally determined by UV photodissociation to decrease from 0.37 eV at $n = 11$ to asymptotically reach 0.22 eV in the limit of very large clusters [97].

As seen in this section, CO_2 cluster anions can serve as excellent examples for how solvation can change the nature of the solute. The subtle balance of electronic stability and solvation energy at play in these systems shows an unexpected richness, which is also observable in other CO_2 containing systems, as some of the later Sections will show.

4. Molecular cluster anions containing CO_2

4.1. *Interaction of CO_2 with halide anions – electrostatics and charge transfer*

The interaction of CO_2 with halide ions is of interest, since (with the exception of fluoride, see below) the excess charge is in this case tightly bound within a closed-shell anion, which is usually not very reactive. This way, the ion-CO_2 interaction is closely related to interaction of a CO_2 molecule with a point charge, and it is interesting from a fundamental point of view to see deviations from this behaviour. Since neutral CO_2 has a positive partial charge on the C atom and negative partial charges on the O atoms, simple electrostatic considerations suggest that the CO_2 molecule will form a Y-shaped complex (C_{2v} symmetry) with a halide ion. The X–C distance in this complex is shorter than the X–O distance, and CO_2 molecule is slightly bent to minimise Coulomb repulsion between the halide ion and the O atoms (see Figure 7).

Photoelectron spectroscopy work carried out by Neumark and coworkers for $X^- \cdot (CO_2)_n$ clusters [115–118] with the heavier halides (X = I, Br, Cl) can give experimental insight into the interactions of halides with CO_2. The photoelectron spectra are characterised by the spin-orbit features of the halogen atoms shifted progressively towards higher electron binding energies due to solvation of the ion by the CO_2 solvent molecules. In addition, vibrational progressions belonging to the bending mode ν_2 of

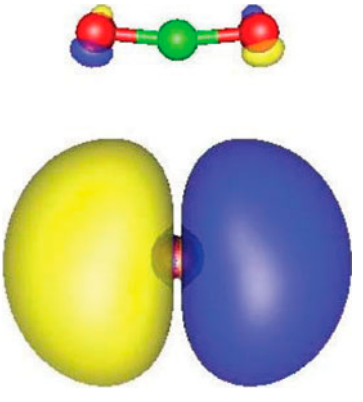

Figure 7. (Colour online) Calculated structure of $Br^- \cdot CO_2$. The blue and yellow shaded regions show the 95% orbital contour of the HOMO. Note the charge transfer to the CO_2 molecule indicated by this contour (see text). The symmetry axis is vertical. The calculations were performed as given in [114].

the CO_2 solvent molecules are observed both in the photoelectron spectra [116–119] and in anion-ZEKE spectra of $I^- \cdot CO_2$ [120], indicating that CO_2 molecules bend in the vicinity of a halide anion, as expected. This leads to dissociation upon photodetachment, and the kinetic energy release into the products depends on the spin-orbit state of the I atom after electron emission [121]. The photoelectron angular distribution and its dependence on detachment energy is only weakly influenced by the presence of a single CO_2 molecule [122].

Electronic structure calculations also find a bent CO_2 structure in such complexes [114,116–118,123–126]. Calculations on the binary complexes $X^- \cdot CO_2$ indicate that the bending of the CO_2 unit (calculated OCO bond angles ranging between 161° for X = Cl and 174° for X = I) is stronger than one would expect based purely by electrostatic interaction with a point charge [114,117,124] (calculated OCO angles 173.7°–176.4°). This implies that some of the excess charge on the halide is transferred onto the CO_2 molecule in the binary cluster. Density functional theory calculations yield natural charges on the CO_2 molecule of −0.0145 e, −0.0413 e and −0.1151 e for X = I, Br and Cl, respectively (B3LYP functional, TZVPP basis sets for all atoms, geometries taken from the calculations described in [114]). The charge transfer to the CO_2 molecules is reflected in the ν_3 vibrational energies (antisymmetric stretching mode), which shift to 2319, 2333 and 2340 cm^{-1} for X = Cl, Br and I, respectively [114]. These small red shifts compared to free CO_2 (where $\nu_3 = 2349 cm^{-1}$ [68]) are caused by accommodation of the excess charge in the antibonding $6a_1$ orbital of the bent CO_2 molecule (see Figure 1). The deformation of CO_2 beyond what would be expected on electrostatic grounds demonstrates that the excess charge is delocalised onto CO_2 despite its negative AEA value.

The sequential shifts of the halide fine structure features in the photoelectron spectra can be used to estimate the stepwise solvation energies by addition of CO_2 solvent molecules. High pressure mass spectrometry experiments by Hiraoka *et al.* [127,128] on $X^- \cdot CO_2$ clusters containing the heavier halide ions (X = I, Br, Cl) yielded binding energies of 200–350 meV for these complexes. For the first few CO_2 solvent molecules, photoelectron spectroscopy results place these energies at 150 meV and 200 meV for X = I and Br, respectively [118]. For the binary $Cl^- \cdot CO_2$ complex, the binding energy obtained from photoelectron spectra is ca. 300 meV [117]. The sequential solvation energies for the first few CO_2 molecules stay nearly constant, but drop substantially after $n = 9$ for X=I and $n = 8$ for X = Br, indicating that the first solvation shell around the halide is filled at these cluster sizes.

Among the halide–CO_2 complexes, fluoride takes a special position, since it does not interact with CO_2 in a weakly bound ion-molecule complex, but rather forms a much stronger C–F bond with mainly covalent character (bond dissociation energy $D_0 = 1.4$ eV [117]) in a molecular anion that could very well be called fluoroformate, $FCOO^-$. This is reflected in the photoelectron spectrum of this ion, which is much more complicated than those of the heavier halide complexes and contains much longer vibrational progressions. According to photoelectron spectroscopy work, electronic structure calculations and Franck–Condon simulations by Neumark and coworkers [117], the OCO bond angle in the anion is 136°. Different from the heavier halides, where the OCO angle after photodetachment moves towards 180°, it becomes smaller upon formation of the $FCO_2^{\bullet}$ radical. The radical can be formed in its $^2B_2$ ground state or in the $^2A_2$ excited state upon photodetachment at 5.8 eV photon energy, with OCO angles of 119° and 125°, respectively.

The series of the halide–CO_2 complexes and clusters shows clearly the change in behaviour of CO_2 from weakly perturbed solvent through various levels of charge transfer between solute ion and solvent, all the way to a reaction partner, becoming part of the solute itself. A very important consequence is that the pseudo-diatomic approximation, i.e. treating the CO_2 molecule as a rare gas atom, is problematic for many, maybe even most situations.

4.2. *Interaction of CO_2 with dihalide anions – solvent–solute interactions in electronic excited states*

There has been an extensive body of work over more than two decades on the interaction of dihalide anions with CO_2, experimentally mostly performed by Lineberger and coworkers [129–143], with theoretical work notably done by Parson and coworkers [135,137–140,142–150] and by McCoy and coworkers [137,142,143,151,152]. In this series of papers, CO_2 had the role of a solvent that could react to electronic excitation of a solvated ion and modify the solute ion's photophysics as well as its vibrational characteristics.

The binding energies of CO_2 molecules to I_2^- are decreasing from ca. 230 meV to ca. 170–180 meV for the first eight CO_2 solvent molecules [130,153]. Their interaction with the ion increases the vibrational frequency of the I_2^- ion in its electronic ground state by several cm^{-1} in $I_2^- \cdot (CO_2)_n$ [154,155]. The blue shift was rationalised by attractive interactions with CO_2 molecules around the I–I bond and charge delocalisation to the solvent, similar to that observed in halide-CO_2 clusters (see Section 4.1). In addition, dephasing of vibrational wavepackets is observed on the ps timescale for the I–I vibration of the solvated ion. However, this dephasing is not associated with fragmentation of the clusters, since no solvent molecules are evaporated during the first few ps after wavepacket excitation [155].

Solvent–solute interaction changes the photophysics in electronic excited states of the solute ion, and the specific properties of CO_2 can play an important role. Early

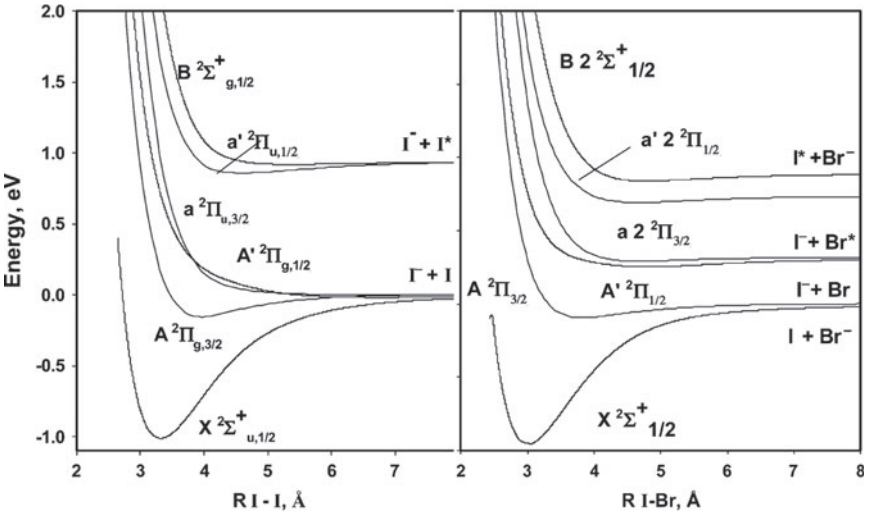

Figure 8. Potential energy surfaces of I_2^- and IBr^-. Reproduced from [137] with permission from the Royal Society of Chemistry.

work [129,130] was performed on photodissociation of $I_2^- \cdot (CO_2)_n$ ions upon excitation from the $X\ ^2\Sigma_u^+$ ground state of the I_2^- chromophore ion to its $A'^2\Pi_{g,1/2}$ state (see Figure 8). The band envelope shifts only weakly upon solvation with CO_2, suggesting that the electronic structure of the solute ion is not significantly perturbed by the presence of CO_2. In bare I_2^-, this transition leads to dissociation into $I^-(^1S_0)$ and $I(^2P_{3/2})$. There are two photodissociation pathways. In one, $I^- \cdot (CO_2)_m$ ions are formed ($m < n$), so the solvated I_2^- parent dissociates upon excitation. Several (on average up to 4) CO_2 solvent molecules are evaporated during the process, accommodating excess vibrational energy. In the second pathway, $I_2^- \cdot (CO_2)_k$ ions are formed ($k < n$), demonstrating that the presence of the solvent can lead to geminate recombination of the nascent $[I^- + I]$ pair by caging. The branching ratio for the two observed pathways changes drastically with cluster size. In small clusters ($n \leq 5$), dissociation is the only observed pathway. The caging fraction then increases smoothly until it reaches 1 at $n = 16$, beyond which it stays constant. Together with mass spectrometry results indicating that $I_2^- \cdot (CO_2)_{16}$ is particularly stable, this suggests that the first solvation shell of I_2^- is filled at cluster size $n = 16$. This size is roughly consistent with the closing of the first solvation shell around CO_2^- in the case of pure $(CO_2)_n$ clusters (see Section 3.2). Qualitatively similar caging is seen for excitation to the $B\ ^2\Sigma_{g,1/2}^+$ state, where spin-orbit relaxation is required in addition to the relaxation processes after lower energy excitations [135,136].

The high caging efficiency at relatively small cluster sizes is surprising, since one may naively expect that there would only be significant caging if the I_2^- parent ion is enclosed or nearly enclosed in the first solvent shell, requiring at least a half-shell or cluster sizes $n > 8$. Parson and coworkers [144–149,156] used non-adiabatic molecular dynamics simulations to trace the high observed caging efficiency in $I_2^- \cdot (CO_2)_n$ clusters to the charge distribution of the excited ion and its polarisation by the solvent. In electronic states with primarily bonding character, the solvent polarises the charge into the most favourably solvated I atom, while the opposite is true in electronic states with primarily antibonding character. The latter behaviour is rather counterintuitive, and the authors termed this 'anomalous charge switching', but it can be understood in terms of state orthogonality in solvated LCAO–MO states [146]. Charge flow is calculated to be anomalous for most internuclear distances in the $A'^2\Pi_{g,1/2}$ state, pushing the charge onto the unsolvated I atom in small clusters upon excitation. During dissociation on the A' surface, the predominantly neutral, solvated I atom collides with the solvent, while the nascent I^- ion is hindered from escaping by the electrostatic and charge transfer interaction with the remaining neutral cluster. Therefore, dissociation on the A' surface is strongly suppressed, leading to the observed caging behaviour, even at small cluster sizes. This behaviour is in contrast with that of more weakly bound $I_2^- \cdot Ar_n$ clusters [134], where the interaction with the solvent is not strong enough to prevent dissociation on the A' surface, since there is only weak electrostatic interaction and no charge transfer component.

Time-resolved photodissociation spectroscopy revealed that the ground state in caged I_2^- is recovered within 30–40 ps for cluster sizes up to $n = 13$, but then drops to shorter times (10–20 ps) for larger clusters [129,130]. The strong cluster size dependence of the cluster dynamics suggests a qualitative change in relaxation dynamics taking place at cluster size $n = 14$, concomitant with the incipient closing of the first solvation shell. Moreover, a recurrence of the ground state absorption is observed [131,132] after 2 ps for large clusters ($n \geq 14$). This feature is a direct result of caging through interaction with the CO_2 solvent [131,132]. Theoretical work [145,147,148]

suggests that caging first leads to recombination of a part of the excited ensemble on the A state, while another part crosses to the ground state at times shorter than 2 ps. The recurrence of absorption can then be traced to transitions from vibrationally excited levels in the electronic ground state to the spin-orbit excited states $a'^2\Pi_{u,1/2}$ and $B\ ^2\Sigma^+_{g,1/2}$ at relatively large internuclear distances. Vibrational relaxation to the solvent prevents the system from revisiting these regions, preventing the recurrence from being repeated. At long times, ground state recovery is reached by electronic quenching of the A state via surface hopping.

Additional work has been performed on the mixed dihalides IX^- (X = Br, Cl, CN) solvated by CO_2 molecules. These systems have a similar electronic structure to I_2^- (see Figure 8) and can serve as test cases for the effects of breaking the symmetry and changing the charge distribution in the ion. Photodissociation of the bare IX^- ion results in I^-, but photodissociation of the CO_2 solvated ion can give rise to ionic photofragments based on I^-, X^- or IX^-. For X = Br [138–143], the bromine atom is preferentially solvated in the ground state. The branching ratio for formation of I^- based products upon excitation to the A' state decreases rapidly with the number of solvent molecules, n, whereas the caging fraction producing IBr^- based ions increases and reaches unity at $n = 8$ (see Figure 9). At intermediate sizes, a small fraction of product ions are Br^- based, which are the result of charge transfer from the I atom to the Br atom on the excited surface. For X = Cl, caging is only observed at intermediate sizes, with a maximum caging fraction of 100% at $n = 3$, but the Cl^- based excited state charge transfer products dominate at larger cluster sizes and the caging fraction drops to zero [133]. Upon excitation to the B state, caging fractions reach significant values only for cluster sizes $N > 10$ [138]. Photodissociation of $ICN^- \cdot (CO_2)_n$ ions results in charge transfer and caging behaviour similar to that of CO_2 solvated ICl^- [151,152]. However, an additional reaction channel may be present in this case due to the possible reaction of a CN^- photoproduct with a CO_2 solvent molecule to form a $[NCCO_2]^-$ ion.

Time-resolved photoelectron spectroscopy [138,139] and photodissociation [140] studies show that although recombination of the IBr^- ion occurs with unit probability for n = 8–10 upon excitation to the A' state, the recombination time is very long

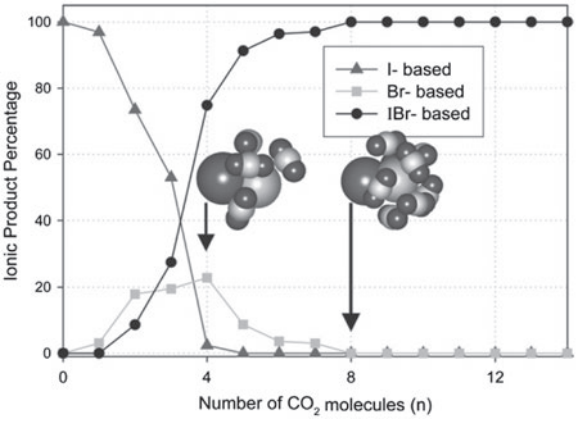

Figure 9. Size evolution of the ionic photoproducts from photodissociation of $IBr^- \cdot (CO_2)_n$ upon excitation to the A' state. Reproduced from [137] with permission from the Royal Society of Chemistry.

(nanoseconds), in contrast to the short recombination time in $I_2^- \cdot (CO_2)_n$ clusters [129,130]. This long recombination time can be traced to the existence of a solvent-induced shallow minimum on the A' surface, trapping the evolving complex. Its depth depends on the asymmetry of the solvent shell, which is largest in the size regime where the recombination time is long. At both smaller and larger cluster sizes ($n \leq 7$, $n \geq 11$), recombination occurs on a picosecond timescale [139]. A detailed, time-resolved photoelectron spectroscopy and quantum dynamics study [142] of the dissociation dynamics of $IBr^- \cdot CO_2$ shows that the solvent plays an important role in the charge transfer process that allows the formation of Br^-. Charge transfer from I^- to Br proceeds via charge delocalisation onto the CO_2 molecule. Immediately upon excitation to the A' state, I^- is formed, and the attractive force between the ion and the CO_2 solvent molecule launches excitation of the $I\cdots CO_2$ stretching vibration. At the inner turning point of this motion, which is first visited at ca. 350 fs after excitation, the energy gap between the A' and the X and A states is at its lowest, comparable with the vibrational energy of the CO_2 bending mode. The slightly bent geometry of the solvent allows the excess electron to delocalise onto the CO_2 molecule to a sufficient degree to facilitate charge transfer to the Br atom, which at this point is ca. 7 Å away from the I atom.

The behaviour of dihalide ions solvated by CO_2 shows how solvent–solute interactions lead to rich photodissociation behaviour and dynamics. The electrostatic interaction of CO_2 with negative charge and the ability of CO_2 to accept charge through bending can lead to subtle modifications of the dihalide excited states giving rise to effects from caging to long-range charge transfer.

4.3. *Hydrated CO_2^- cluster anions*

The reduction of CO_2 in aqueous solution or at the interface of water is an important process in the context of the regeneration of chemical fuels from CO_2 [4]. Of interest here are reactions of hydrated electrons with CO_2 and the solvation of CO_2^- by water.

Experiments by the groups of Johnson and of Beyer showed that collisions of CO_2 with water cluster anions, $(H_2O)_n^-$ result in the uptake of CO_2 and subsequent loss of water molecules [157–159] in the reaction

$$(H_2O)_n^- + CO_2 \rightarrow CO_2^- \cdot (H_2O)_p + (n-p)H_2O; \quad (n-p) \approx 2-3. \tag{4}$$

Successive evaporation of water molecules by blackbody induced dissociation of the clusters produces clusters with sizes down to $p = 2$, although even the monohydrate ion $CO_2^- \cdot H_2O$ has been observed in mass spectrometry experiments [160]. Upon uptake and reduction of CO_2, the product clusters can react further via

$$CO_2^- \cdot (H_2O)_p + O_2 \rightarrow O_2^- \cdot (H_2O)_{p-x} + CO_2 + xH_2O; \quad x \approx 3-4, \tag{5}$$

and this reaction has been invoked as a possible mechanism for the formation of atmospheric superoxide [76]. Although the strong interaction between CO_2 and superoxide makes a direct charge transfer between these species without formation of the CO_4^- ion doubtful (see Section 4.4), water clusters could serve as mediators for such charge transfer processes. Interestingly, the reverse is true for the reaction of O_2^- with CO_2, as Castleman and coworkers found that hydration by only a few water molecules strongly inhibits the reaction of O_2^- with CO_2 [161], presumably because of the strong coordination of superoxide with its first hydration shell [162].

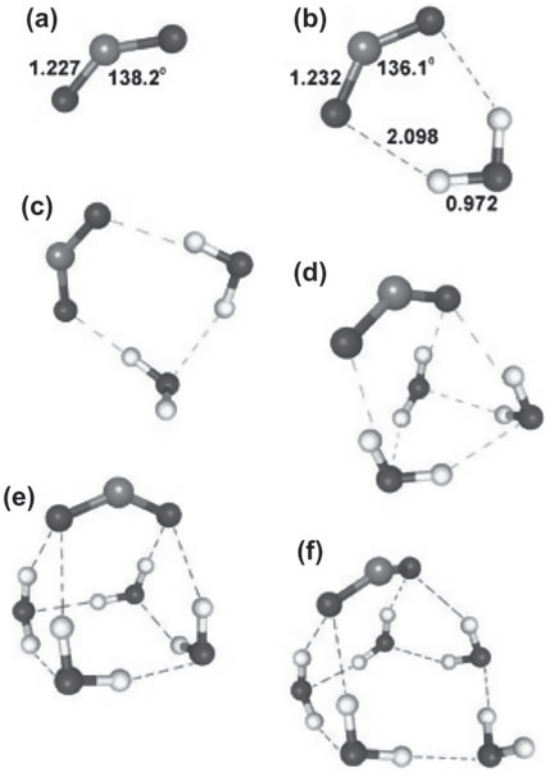

Figure 10. Calculated structures of $CO_2^- \cdot (H_2O)_n$ cluster ions. Reproduced with permission from [159], copyright (2004), Wiley-VCH Verlag GmbH & Co. KGaA.

Beyer and coworkers showed that collisions of hydrated CO_2^- cluster ions with CH_3SH lead to the generation of formate anions, $HCOO^-$ [163,164]. The formation of C–C bonds in reactions of hydrated CO_2^- containing cluster ions has also been found [165–167]. With some other reactants (e.g. nitromethane), the role of CO_2^- is that of a reducing agent [168].

At the heart of the reactivity of hydrated CO_2^- is of course the electronic structure and hydrogen bonding environment of CO_2^- in such clusters. Quantum chemical calculations indicate [159,169] that a single water molecule can interact with CO_2^- by forming two H-bonds, similar to the monohydrates of other triatomic anions or anionic domains of larger molecules [170] (see Figure 10). At higher levels of hydration, these calculations show that water molecules tend to form networks, leaving the CO_2^- ion on the surface of that network, again similar to the hydration of many other anions [20]. Infrared spectroscopy experiments by Nagata and coworkers on $CO_2^- \cdot CO_2 \cdot (H_2O)_2$ did not show evidence of the water–water H-bond that one would expect for this cluster [169], but the influence of the second CO_2 may hinder the formation of the network, or the water–water H-bond may be disrupted by too high a temperature [171]. So far, there are no infrared spectroscopy data available on $CO_2^- \cdot (H_2O)_n$ clusters with more than two water molecules.

Work by Sanov and coworkers showed that the photoelectron angular distributions upon electron detachment from hydrated CO_2^- at 355 nm (3.49 eV) dramatically

decrease in anisotropy as the number of water molecules is increased beyond three [172]. Quantum chemical calculations suggest that the character of the charge carrier remains CO_2^-, independent of the level of hydration (at least for small clusters). Rather than by a change in the electronic character of the charge carrier, the change in photoelectron angular distributions has been explained by a hydration-stabilised excited state in the cluster, followed by autodetachment. The same excitation energy can lead to photodissociation of the CO_2^- ion [173,174], resulting in $O^- \cdot (H_2O)_k$ ions ($k < n$). The presence of a second (neutral) CO_2 molecule in the water cluster can give rise to fragments of the type $CO_3^- \cdot (H_2O)_k$ as the nascent O^- ion reacts with the second CO_2 molecule to form hydrated CO_3^- [173,174]. The excited state giving rise to this rich behaviour has been assigned to the $^2A_1 \rightarrow {}^2B_1$ transition [174] observed for CO_2^- in crystalline matrices [32,69]. The dissociation was attributed to the evolution of the system through a Renner–Teller intersection with the ground state, followed by its dissociation [175]. Similar photodissociation processes observed at 266 nm (4.66 eV) excitation is believed to proceed via a conical intersection of the second and third excited states of CO_2^- [175]. Interestingly, CO_2 can be taken up by a water cluster anion *without* forming a CO_2^- ion at first, if the uptake proceeds at sufficiently low temperatures and the reactants can be frozen out in the entrance channel of the reaction [176]. In this case, infrared excitation of either the water cluster or the neutral CO_2 can result in exothermic formation of CO_2^-, concomitant with the evaporation of two water molecules.

Water can also be the minority species in clusters of the form $[(CO_2)_n(H_2O)_m]^-$ ($m < n$). In this case, the question is how the presence of water molecules affects the subtle balance between electronic stability and solvation energy in neat $(CO_2)_n^-$ clusters, and whether it changes the nature of the charge carrier (see Section 3.2). The Nagata and Johnson groups have performed infrared and photoelectron spectroscopy experiments on such clusters [169,177]. They found that a single water molecule binds to the charge carrier in the cluster. The $C_2O_4^-$ core ion is still the dominant structural motif for small clusters ($n = 2$ and 3), with the water molecule bridging across two O atoms. The CO_2^- monomer ion is the preferred charge carrier at $n > 4$, with both motifs coexisting at $n = 4$. In contrast, this core ion change occurs at $n = 6$ in neat $(CO_2)_n^-$ ions (see Section 3.2). The presence of the water molecule and its ability to form two strong H-bonds with a CO_2^- ion helps to localise the charge in a single CO_2 unit and precipitates the early change of the charge carrier motif. Interestingly, replacing water with methanol as the perturbing molecule in the cluster, the $C_2O_4^-$ core ion exists only for $[(CO_2)_2 \cdot CH_3OH]^-$ [178,179], while all other cluster sizes seem to exhibit a CO_2^- charge carrier. While the presence of one or two water molecules in CO_2 cluster anions changes the switching point between monomer and dimer cores, it does not significantly change the shape of the HOMO in either core, as was shown by photoelectron imaging spectroscopy experiments [109].

It seems that the key to the chemistry of hydrated CO_2^- lies in the efficient stabilisation of the CO_2^- by the water network by just the right amount without hindering charge transfer and subsequent reactions.

4.4. *Reaction products of non-hydrated CO_2^-*

Anion-CO_2 interactions can go beyond solvation and result in reaction with other species, as mentioned above in Section 4.1 for the case of the reaction of fluoride with CO_2, resulting in the formation of fluoroformate. Some more examples were discussed

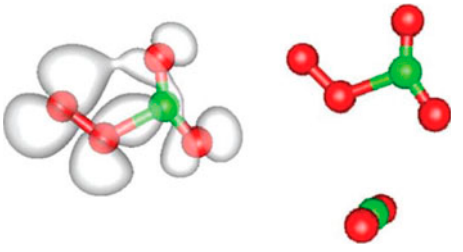

Figure 11. (Colour online) Calculated structures of CO_4^- with its HOMO (left) and of $CO_4^- \cdot CO_2$ (right). Carbon atoms are shown in green, oxygen atoms in red. Structures shown here were calculated with the methods used in [181].

in Section 4.3, looking at reactions of hydrated CO_2^- . In this Section, we will review reactions of CO_2, CO_2^- and $(CO_2)_n^-$ with some selected molecular partners.

The interaction of O_2^- is one such example. High-pressure mass spectrometry experiments by Hiraoka and Yamabe [180] found that the binding energy of $O_2^- \cdot CO_2$ is 0.82 eV, which is too high to be consistent with an ion–molecule complex, and suggests that there is a chemical bond between the two moieties. In contrast, the binding energy of subsequent CO_2 units in clusters of the form $[O_2(CO_2)_n]^-$ is nearly a factor of three lower than that of the first CO_2. The charge carrier in such clusters can therefore be assumed to be of the form CO_4^-.

The geometry of CO_4^- is planar in the ground state, with a C–O σ bond connecting the CO_2 moiety to the O_2 moiety (see Figure 11). This structure can be qualitatively understood based on orbital interaction arguments describing the charge transfer to the CO_2 unit [180]. An alternative explanation is that the C–O σ bond forms by 'docking' the C atom to the π^* orbital of O_2^-, the latter providing a structured charge distribution in contrast to the spherical charge distribution of a halide ion [181]. Torsion of the O_2 moiety about its bond with the carbon atom results in a second isomer calculated to be ca. 130 meV higher in energy than the ground state [181]. The CO_2 unit in CO_4^- is

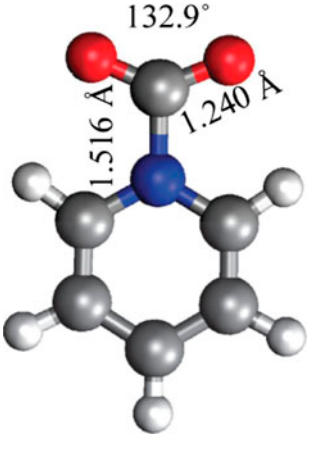

Figure 12. (Colour online) Calculated structure of $C_5H_5NCO_2^-$. Adapted with permission from [110], copyright (2010) American Chemical Society.

strongly bent at 143°, based on density functional theory calculations as used in [181], consistent with strong calculated charge transfer (around −0.5 e). The CO_4^- ion has been observed in matrix isolation infrared spectroscopy studies [33,34,182], and its vibrational signatures are consistent with harmonic calculations of the infrared spectrum of CO_4^- in planar geometry [33]. Similarly, an infrared photodissociation study of $[O_2(CO_2)_n]^-$ was consistent with anharmonic calculations of the infrared spectrum of planar CO_4^- [181]. The arrangement of the solvent CO_2 molecules is governed by electrostatic interactions, where neighbouring solvent molecules preferentially align themselves perpendicular to each other with the C atoms in the plane of the CO_4^- ion [181] (see Figure 11).

An analogous reaction of $(CO_2)_n^-$ clusters with NO yields $ONCO_2^-$ ions by radical addition, as studied by photoelectron spectroscopy and *ab initio* calculations [183]. Interestingly, docking at the N atom is preferred in this case, and the NO moiety is not in the CO_2 plane, in contrast to the structure of CO_4^-.

A very interesting reaction is that of pyridine with CO_2 cluster anions, yielding covalently bound carbamate ions $C_4H_4NCO_2^-$ (see Figure 12), solvated by additional CO_2 molecules [110,184]. This molecule is of interest in the context of catalytic reduction of CO_2 in aqueous solutions, using pyridine-based species as catalysts [8]. Here, a planar molecular ion with a C–N σ bond and a strongly bent CO_2 functional group is formed. Photoelectron spectroscopy [184] and infrared photodissociation spectroscopy results [110] corroborate this structure, and the excess charge is delocalised over the molecule. The barrier for torsion around the C–N bond axis is calculated to be ca. 0.7 eV [184], and it is assumed that this high barrier is caused by a weak π contribution to the C–N bond, which would be consistent with the charge delocalisation in an extended π network in the anion. Infrared spectra of $[C_4H_4N(CO_2)_n]^-$ cluster ions suggest that not all collisions of $(CO_2)_n^-$ ions with pyridine result in reactions, but that a small fraction of these clusters remains trapped in the entrance channel of the reaction leading to the $C_4H_4NCO_2^-$ product ion [110].

Extension to aromatic species with more than one N atom leads to formation of up to two C–N bonds if the N atoms in the ring are not direct neighbours [185]. Only one of two neighbouring N atoms can undergo C–N bond formation due to steric hindrance. Similar to the case of pyridine–CO_2 cluster anions, the excess charge is delocalised over the whole π system of the molecule, including the two CO_2 units. This delocalisation is concomitant with a drastic increase in electron binding energy, and photoelectron spectra have been used to prove the stepwise formation of the covalent C–N bonds by observing the increase of electron affinities upon bond formation and delocalisation [185]. Analogous experiments with 2-aminopyridine revealed C–N bond formation and delocalisation of the excess charge into an extended π system despite the steric hindrance by the neighbouring amino group [186].

Reactions of $(CO_2)_n^-$ clusters with methyl iodide can lead to a variety of products [187,188]. In principle, one could expect a charge transfer reaction to lead to product ions that are based on I^-, given the tendency of CH_3I to attach electrons dissociatively. However, mass spectrometry shows that the major products are clusters of the form $[(CO_2)_nCH_3I]^-$. For $n = 1$–3, the charge carrier in the clusters was identified to be acetyloxy iodide, $CH_3CO_2I^-$, where the iodine atom is bound through an O–I bond [187]. In contrast, large clusters ($n \geq 7$) have CO_2^- as a charge carrier, so CH_3I is incorporated into the cluster, but does not react. Interestingly, the intermediate cluster size regime $4 \leq n \leq 6$ do not exist. A possible explanation of this 'gap' in the size distribution is that larger clusters first incorporate a CH_3I molecule and cool by CO_2 monomer

evaporation. If this results in a sufficiently small cluster ($n = 6$), the residual energy in the system is enough to facilitate the reaction to form acetyloxy iodide, and the exothermicity of the reaction leads to further evaporation of CO_2 molecules, resulting in the absence of certain cluster sizes.

All these studies show that CO_2^- is a versatile reaction partner. As a consequence, one-electron reduction of CO_2 can turn this molecule from a pollutant into a valuable resource. In view of the complexity of electrochemical processes yielding CO_2^- in the condensed phase and the concomitant difficulties of *in situ*-measurements, cluster studies can uncover important information on how to understand catalysts for such reaction processes. The next section is focused on this topic.

5. Anionic complexes of CO_2 with transition metals

Nearly two decades ago, the oxidation of CO by metal catalysts received enormous attention. In this context, much work focused on gold clusters and nanoparticles, particularly based on the work of Haruta and coworkers [26,27,189] and of Heiz and coworkers [190–192]. This work also inspired work on cluster anions *in vacuo* on the oxidation of CO by gold containing species [193,194].

More recently, the reduction of CO_2 instead of the oxidation of CO has come increasingly into the focus of designing and understanding catalyst species [4] in electrochemical or photoelectrochemical schemes (see, e.g. [1–3,5–8,10,11]). Metal-CO_2 interactions are particularly interesting in the context of catalytic reduction of CO_2 with the aim of generating feedstock for chemical fuels or other carbon-based chemicals

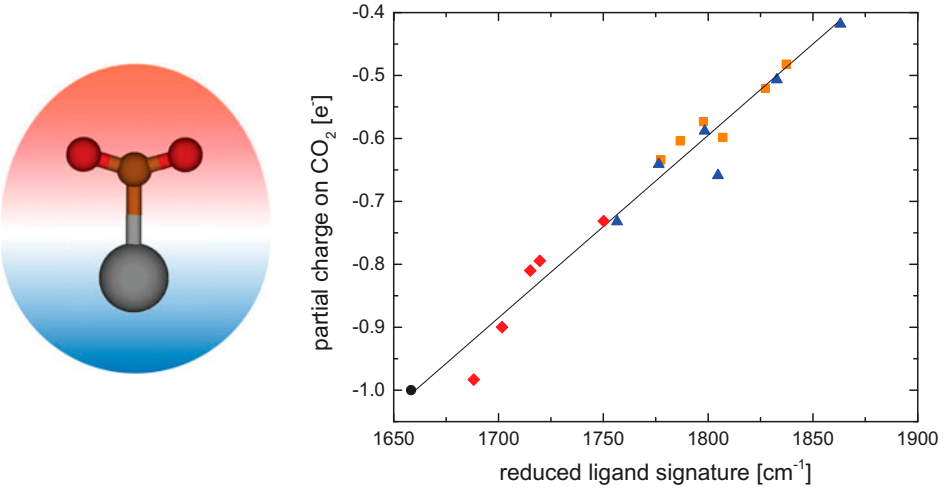

Figure 13. (Colour online) Left: Metalloformate structure of MCO_2^- complexes (M = Au, Ag, Cu). The red and blue shaded regions show regions where solvation by additional CO_2 molecules leads to red and blue shifts of the antisymmetric CO stretching mode of the complex (see text for discussion). Right: Calculated charge on the CO_2 moiety of metalloformate complexes as a function of the experimentally measured antisymmetric CO stretching mode, compiled from [111,198] and from calculations performed in [199]. Orange squares, blue triangles and red diamonds reflect data for Au, Ag and Cu, respectively, at different levels of solvation. The black circle represents the antisymmetric stretching mode of CO_2^- in a Ne matrix [34]. The full line is a linear fit through the data.

from CO_2. Since reduction of CO_2 requires the transfer of electrons and protons [4], the interaction of CO_2 with negative charge is an obvious starting point for a mechanistic understanding of CO_2 reduction catalysts. Some very interesting organic catalysts without transition metal centres have been proposed for CO_2 reduction, for example in work by Bocarsly and coworkers and by Carpenter and coworkers [8,9]. However, most candidates for CO_2 reduction catalysts are based on transition metals, either as metal atoms embedded in organic frameworks [10,195,196] or supported as clusters and nanoparticles on surfaces [10]. In the former case, the metal species is typically a positive ion. In surface supported catalysts, the situation is less clear, but it seems that the catalytically active sites are likely corners or edges, which can serve as concentration points for charge density, making them more reactive than flat facets of simple polycrystalline metals (see, e.g. [10,197]). It is therefore interesting to understand transition metals in anionic complexes with CO_2, since these complexes can serve as model systems for the interaction of CO_2 with active sites on supported reduction catalysts.

Recent infrared spectroscopic work by Weber and coworkers has focused on the interaction of CO_2 with various metal atoms in singly negatively charged clusters of the form $[M(CO_2)_n]^-$ with M = Au, Ag, Cu, Co and Ni [111,198–202]. This set of studies contrasts two different transition metal families, the coinage metals (Cu, Ag, Au) and first row transition metals (here: Co, Ni, Cu), with copper being a member of both families.

There are several structural motifs in anionic metal-CO_2 complexes, and they vary strongly between noble metals and open-d-shell metals. The complexes of CO_2 with silver and gold are governed by binary complexes $M\,CO_2^-$ which can be characterised as metalloformates [111,198–200], i.e. formate ions where the H-atom has been replaced by a metal atom (see Figure 13). These complexes form weak M-C σ bonds with calculated binding energies of 0.2–0.4 eV [111,198,200]. Copper also forms formate-type complexes, although these do not seem to be the dominant structural motif in $[Cu(CO_2)_n]^-$ clusters [199]. Metalloformate-type complexes are denoted η^1 type complexes in the organometallic chemistry literature, although they have only rarely been observed, and usually only with a single CO_2 ligand among several other ligands [203].

The excess negative charge in metalloformate complexes MCO_2^- is delocalised over the whole ion. This is very interesting in the context of CO_2 reduction catalysis, as the charge on the activated CO_2 ligand may be a figure of merit for evaluating the suitability of a particular catalyst material. The amount of charge on the CO_2 ligand is strongly dependent on the metal and on the solvation environment of the complex (see Figure 13). Generally, the amount of excess charge on the partially reduced CO_2 ligand follows the trend Au < Ag < Cu. This behaviour can be explained by the electronegativities of the coinage metal atoms, which decrease from Au to Cu. In addition, solvation of the complex by CO_2 molecules polarises the complex. Solvation of the CO_2 ligand serves to increase the negative charge in the partially reduced ligand, increasing reductive activation, while solvation of the metal atom increases the charge on the metal atom (see Figure 13). The latter has been observed only in auroformate complexes [198], while metalloformate complexes of silver and copper are selectively solvated on the side of the activated CO_2 ligand [111,199]. This allows the conclusion that the gold complexes are embedded in CO_2 clusters of sufficient size, while MCO_2^- complexes stay on the surface of CO_2 clusters for M = Ag, Cu. Interestingly, there is a near-linear correlation between the calculated partial charge (following a natural populations analysis) on the activated CO_2 ligand and the antisymmetric CO stretching

frequency, which is independent of the nature of the metal partner, hinting that this correlation may be a universal property of reductively activated CO_2 in metalloformate complexes (see Figure 13). We note that for lesser amounts of charge transfer to a CO_2 molecule close to the anion, the relationship shown in Figure 13 deviates significantly from linearity, for example in halide-CO_2 complexes.

There are some peculiar observations in the noble metal complexes with CO_2 . In $[Au(CO_2)_n]^-$ complexes, there is a single cluster size, $n = 8$, where no signature of a partially reduced CO_2 ligand is observed at all [198]. The solvated species seems to be Au^- instead of $AuCO_2^-$. This is reminiscent of the core ion switching observed in $(CO_2)_n^-$ ions (see Section 3.2). It is plausible that the first solvation shell of Au^- is filled at $n = 8$, since the Au^- ion is of similar size as the Br^- ion, which in turn closes its first solvation shell at this size [118]. While in $(CO_2)_n^-$ ions, there are several cluster sizes showing a preference for a smaller charge carrier ($n = 6$–13), the size region in which a smaller solute ion is preferred due to solvation energy shrinks in $[Au(CO_2)_n]^-$ cluster ions to a single cluster size.

In $[Ag(CO_2)_n]^-$ complexes, we are faced with the opposite observation. Here, the metal atom can act as a spectator, i.e. it can be part of the cluster without being part of the charge carrier. Apart from the metalloformate motif, cluster sizes $n = 3$–9 also exhibit the infrared signatures of CO_2^- and $C_2O_4^-$ ions, showing that CO_2-based charge carriers can exist in the presence of the silver atom in theses systems. This can be traced to a robust minimum in the potential energy surface, which is calculated to be ca. 0.5 eV higher in energy than the solvated argentoformate complex in the case of $n = 4$ [111]. This minimum represents a possible pathway for the separation of a nascent CO_2-based charge carrier from the catalyst upon reduction.

The interactions of CO_2 with metals that have open d-shells in anionic complexes are fundamentally different in nature from the metalloformate complexes [199,201,202]. The species studied so far (containing Co, Ni or Cu) predominantly form metallate complexes with positively charged metal centres and typically two negatively charged CO_2 ligands that interact with the metal in a bidentate structural motif (see Figure 14). The angle between the OCO planes of the CO_2 ligands varies with the metal. The bindentate interaction motif has been denoted η^2 in the organometallic literature and is much more pervasive than the η^1 motif. However, in most CO_2-containing metal complexes synthesised in the condensed phase, there is usually no more than one CO_2 ligand bound to the metal centre, and the other coordination positions are filled with bulkier ligands [203].

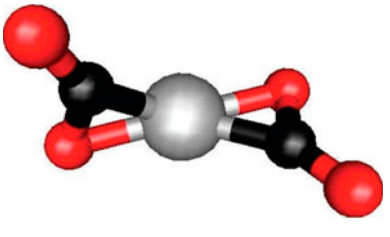

Figure 14. (Colour online) Bidentate interaction motif of the $[CO_2MCO_2]^-$ charge carrier found in $[M(CO_2)_n]^-$ cluster ions with M = Co, Ni, Cu [199,201,202]. The metal atom is shown in gray, C atoms are black and O atoms are red. The actual structure shown is for M = Co and was obtained using the methods given in [201]. The angle between the two OCO planes depends on the metal centre.

Interestingly, although there are calculated structures that are based on the insertion of the metal atom into a C–O bond, this structural motif is a minor contributor to the observed spectra, even if they often represent the lowest energy isomers found in calculations [199,201,202,204]. It is assumed that there is a high barrier towards formation of these isomers, hindering the insertion reaction.

The solvent response of the bidentate metallate motif depends on the metal. While $[Co(CO_2)_2]^-$ shows no significant structural changes as a function of solvation [201], analogous Ni complexes show small splitting and shifts of the CO stretching frequencies, revealing a softer core ion, where different solvent isomers lead to small changes in the charge distributions and result in different infrared signatures [202]. This is even more pronounced in $[Cu(CO_2)_2]^-$, where solvation of the core ion with four or more CO_2 molecules results in significant spectral congestion [199]. The binding energies of the CO_2 ligands to the metal centres in the metallate complexes are of the order of 1–2 eV [199,201,202], much higher than in the metalloformates.

A special case that should be mentioned here are complexes of the form $[V(CO_2)_n]^+$, studied by Duncan and coworkers [112] using infrared photodissociation spectroscopy. While the complex as a whole is *positively* charged, the signatures of the $C_2O_4^-$ ion appear in spectra with $n \geq 7$. This suggests that there is a solvent-driven intracluster reaction resulting in the formation of a V^{2+} metal ion and a $C_2O_4^-$ anion. The reaction is likely brought about by a metal-to-ligand electron transfer reaction, which is driven by a combination of the creation of an expanded coordination sphere around the V^{2+} dication, electrostatic attraction between the hexa-coordinated dication and the nascent $C_2O_4^-$ anion, and the solvation energy of the two ionic species. Other transition metal systems interacting with CO_2 could possible exhibit similar behaviour.

Similar to the $[M(CO_2)_n]^-$ model systems described above, anions of metal oxides and metal clusters and their interactions with CO_2 are of great interest to understand the function of CO_2 reduction catalysts. Reactions with cluster anions of Pd, Pt and Ni reveal that several CO_2 molecules are readily attached to clusters, and that even reactions forming CO occur in the case of Ni_n^- clusters [205]. Jarrold and coworkers found that group 6 suboxide cluster anions of the form $M_xO_y^-$ (M = Mo, W) are sequentially oxidised by reactions with CO_2 [206–208], and calculations suggested the formation of new M–O bonds together with a weakly bound CO molecule.

The studies reviewed here show that transition metal complexes with CO_2 reveal a great variability of CO_2 as a ligand. The η^2 motif involving two CO_2 ligands represents new chemistry. There is great potential for new observations in studying such complexes with more transition metals, and our molecular-level understanding of CO_2 reduction catalysts is bound to profit from such work.

6. Outlook and future challenges

Anionic CO_2 containing systems continue to present interesting future challenges, both in the case of CO_2 containing clusters and for molecular ions. Even some of the basic molecular properties, such as the AEAs of CO_2 and C_2O_4 are still unknown. This is owing to the strong geometry change between the neutral and anionic systems. In the case of CO_2^-, an additional difficulty lies in the short lifetime of the anion against autodetachment. Only the VDE is known for either system, whereas the AEA values are only estimates. Vibrationally well resolved photoelectron spectra in concert with high-level quantum chemical calculations and the resulting Franck–Condon simluations could lead to an improved value for both of these systems. The SEVI technique,

developed about 10 years ago by Neumark and coworkers [119] would probably be the experimental method of choice in this regard.

Experiments on $(CO_2)_n^-$ cluster ions where either the neutral precursor is prepared in a well-defined state, or where the nascent cluster ion prepared with well-defined electron kinetic energy during the attachment process could connect electron attachment and spectroscopy of such anions and result in a better understanding of the attachment process.

The interaction of CO_2 with reduction catalysts is particularly fascinating. The understanding of the molecular properties of transition metal complexes involving CO_2 as a ligand may serve to provide us one day with the ability to rationally design catalysts for CO_2 reduction based on cost-effective transition metals (as opposed to the currently identified platinum group catalysts) and enable the implementation of an affordable carbon-neutral fuel cycle. Advances in cryogenic ion spectroscopy (e.g. [209–212]) are particularly well suited to understand such organometallic complexes. Complexes of CO_2 with metal oxide anions are similarly interesting in this regard, as are catalysts that are not based on transition metals, which may enable the construction of artificial leaves [9].

In closing, there is no shortage of interesting and challenging topics in the area of cluster studies on the interaction of CO_2 with negative charge, and in addition to gratifying scientific insight, great and potentially transformative benefits are within reach.

Acknowledgement

The author gratefully acknowledges support from the National Science Foundation [Grant PHY-1125844] and helpful discussion with Benjamin J. Knurr.

References

[1] W. Rüttinger and G.C. Dismukes, Chem. Rev. **97**, 1 (1997).
[2] M. Yagi and M. Kaneko, Chem. Rev. **101**, 21 (2001).
[3] J.H. Alstrum-Acevedo, M.K. Brennaman, and T.J. Meyer, Inorg. Chem. **44**, 6802 (2005).
[4] Y. Hori, in *Modern Aspects of Electrochemistry*, edited by C.G. Vayenas, R.E. White and M.E. Gamboa-Aldeco (Springer, New York, 2008), Vol. 42, pp. 89–189.
[5] X. Sala, I. Romero, M. Rodríguez, L. Escriche, and A. Llobet, Angew. Chem. - Int. Ed. **48**, 2842 (2009).
[6] J.J. Concepcion, J.W. Jurss, M.K. Brennaman, P.G. Hoertz, A.O.T. Patrocinio, N.Y.M. Iha, J.L. Templeton, and T.J. Meyer, Acc. Chem. Res. **42**, 1954 (2009).
[7] H. Dau, C. Limberg, T. Reier, M. Risch, S. Roggan, and P. Strasser, ChemCatChem. **2**, 724 (2010).
[8] E. Barton Cole, P.S. Lakkaraju, D.M. Rampulla, A.J. Morris, E. Abelev, and A.B. Bocarsly, J. Am. Chem. Soc. **132**, 11539 (2010).
[9] R.D. Richardson, E.J. Holland, and B.K. Carpenter, Nature Chem. **3**, 301 (2011).
[10] Y.H. Chen, C.W. Li, and M.W. Kanan, J. Am. Chem. Soc. **134**, 19969 (2012).
[11] L. Zhang, D. Zhu, G.M. Nathanson, and R.J. Hamers, Angew. Chem. Int. Ed. **53**, 9746 (2014).
[12] A.W. Castleman, and S. Wei, Annu. Rev. Phys. Chem. **45**, 685 (1994).
[13] J.M. Lisy, Int. Rev. Phys. Chem. **16**, 267 (1997).
[14] M.A. Duncan, Annu. Rev. Phys. Chem. **48**, 69 (1997).
[15] Q. Zhong and A.W. Castleman, Chem. Rev. **100**, 4039 (2000).

[16] C. Dedonder-Lardeux, G. Grégoire, C. Jouvet, S. Martrenchard, and D. Solgadi, Chem. Rev. **100**, 4023 (2000).
[17] J.V. Coe, Int. Rev. Phys. Chem. **20**, 33 (2001).
[18] D.M. Neumark, Annu. Rev. Phys. Chem. **52**, 255 (2001).
[19] X.B. Wang, X. Yang, and L.S. Wang, Int. Rev. Phys. Chem. **21**, 473 (2002).
[20] W.H. Robertson and M.A. Johnson, Annu. Rev. Phys. Chem. **54**, 173 (2003).
[21] J.M. Farrar, Int. Rev. Phys. Chem. **22**, 593 (2003).
[22] O. Dopfer, Int. Rev. Phys. Chem. **22**, 437 (2003).
[23] E.J. Bieske, Chem. Soc. Rev. **32**, 231 (2003).
[24] X.B. Wang and L.S. Wang, Annu. Rev. Phys. Chem. **60**, 105 (2009).
[25] K.R. Asmis and D.M. Neumark, Accounts Chem. Res. **45**, 43 (2012).
[26] M. Haruta, Catal. Today. **36**, 153 (1997).
[27] M. Haruta, Nature. **437**, 1098 (2005).
[28] A.D. Walsh, J. Chem Soc. 1953, 2266.
[29] T. Sommerfeld, H.D. Meyer, and L.S. Cederbaum, Phys. Chem. Chem. Phys. **6**, 42 (2004).
[30] G. Herzberg, *Molecular Spectra and Molecular Structure*, Vol III. (Krieger Publishing, Malabar, FL, 1991).
[31] D.W. Ovenall and D.H. Whiffen, Mol. Phys. **4**, 135 (1961).
[32] K.O. Hartman and I.C. Hisatsun, J. Chem. Phys. **44**, 1913 (1966).
[33] M.F. Zhou and L. Andrews, J. Chem. Phys. **110**, 2414 (1999).
[34] W.E. Thompson and M.E. Jacox, J. Chem. Phys. **111**, 4487 (1999).
[35] G.L. Gutsev, R.J. Bartlett, and R.N. Compton, J. Chem. Phys. **108**, 6756 (1998).
[36] M.E. Jacox and D.E. Milligan, Chem. Phys. Lett. **28**, 163 (1974).
[37] Z.H. Kafafi, R.H. Hauge, W.E. Billups, and J.L. Margrave, Inorg. Chem. **23**, 177 (1984).
[38] M.E. Jacox and W.E. Thompson, High Temp. Sci. **28**, 225 (1989).
[39] M.F. Zhou and L. Andrews, J. Chem. Phys. **110**, 6820 (1999).
[40] S.T. Arnold, J.V. Coe, J.G. Eaton, C.B. Freidhoff, L.H. Kidder, G.H. Lee, M.R. Manaa, K.M. McHugh, D. Patel-Misra, H.W. Sarkas, and J.T. Snodgrass, K. H. Bowen, in *Proceedings of the Enrico Fermi International School of Physics, CVII Course, Varenna*, edited by G. Scoles (North-Holland, Amsterdam, 1989), pp. 467–490.
[41] R.N. Compton, P.W. Reinhardt, and C.D. Cooper, J. Chem. Phys. **63**, 3821 (1975).
[42] J. Pacansky, U. Wahlgren, and P.S. Bagus, J. Chem. Phys. **62**, 2740 (1975).
[43] W.B. England, B.J. Rosenberg, P.J. Fortune, and A.C. Wahl, J. Chem. Phys. **65**, 684 (1976).
[44] D.G. Hopper, Chem. Phys. **53**, 85 (1980).
[45] W.B. England, Chem. Phys. Lett. **78**, 607 (1981).
[46] T. Sommerfeld, J. Phys. B - At. Mol. Opt. Phys. **36**, L127 (2003).
[47] C.D. Cooper, and R.N. Compton, J. Chem. Phys. **59**, 3550 (1973).
[48] M. Knapp, O. Echt, D. Kreisle, T.D. Märk, and E. Recknagel, Chem. Phys. Lett. **126**, 225 (1986).
[49] M.K. Raarup, H.H. Andersen, and T. Andersen, J. Phys. B - At. Mol. Opt. Phys. **32**, L659 (1999).
[50] D. Schröder, C.A. Schalley, J.N. Harvey, and H. Schwarz, Int. J. Mass Spec. **185**–**187**, 25 (1999).
[51] R. Middleton and J. Klein, Phys. Rev. A. **60**, 3786 (1999).
[52] P.D. Burrow and L. Sanche, Phys. Rev. Lett. **28**, 333 (1972).
[53] M.J.W. Boness and G.J. Schulz, Phys. Rev. A. **9**, 1974, 1969.
[54] M.A. Morrison, Phys. Rev. A. **25**, 1445 (1982).
[55] K.H. Kochem, W. Sohn, N. Hebel, K. Jung, and H. Ehrhardt, J. Phys. B - At. Mol. Opt. Phys. **18**, 4455 (1985).
[56] H. Estrada, and W. Domcke, J. Phys. B - At. Mol. Opt. Phys. **18**, 4469 (1985).
[57] L.A. Morgan, Phys. Rev. Lett. **80**, 1873 (1998).
[58] T.N. Rescigno, D.A. Byrum, W.A. Isaacs, and C.W. McCurdy, Phys. Rev. A. **60**, 2186 (1999).

[59] M. Allan, Phys. Rev. Lett. **87**, 033201 (2001).
[60] D. Field, N.C. Jones, S.L. Lunt, and J.P. Ziesel, Phys. Rev. A. **64**, 022708 (2001).
[61] R.K. Nesbet, S. Mazevet, and M.A. Morrison, Phys. Rev. A. **64**, 033201 (2001).
[62] M. Allan, J. Phys. B - At. Mol. Opt. Phys. **35**, L387 (2002).
[63] M. Allan, Phys. Scripta. **110**, 161 (2004).
[64] W. Vanroose, Z.Y. Zhang, C.W. McCurdy, and T.N. Rescigno, Phys. Rev. Lett. **92**, 053201 (2004).
[65] M. Lezius, T. Rauth, V. Grill, M. Foltin, T.D. Märk, and Z. Phys, D. **24**, 289 (1992).
[66] S. Denifl, V. Vizcaino, T.D. Märk, E. Illenberger, and P. Scheier, Phys. Chem. Chem. Phys. **12**, 5219 (2010).
[67] R. Dressler and M. Allan, Chem. Phys. **92**, 449 (1985).
[68] T. Shimanouchi, *Tables of Molecular Vibrational Frequencies Consolidated Volume I*, (National Bureau of Standards, 1972).
[69] G.W. Chantry and D.H. Whiffen, Mol. Phys. **5**, 189 (1962).
[70] J. Keene, Y. Raef, and A. Swallow, in *Pulse Radiolysis*, edited by M. Emert, J. Keene and J.P. Swallow (Academic Press, London, 1965), p. 99.
[71] M.A. Johnson and W.C. Lineberger, in *Techniques for the Study of Gas-Phase Ion Molecule Reactions*, edited by J.M. Farrar and W. Saunders (Wiley, New York, 1988), p. 591.
[72] K. Takahashi, S. Sawamura, N.M. Dimitrijevic, D.M. Bartels, and C.D. Jonah, J. Phys. Chem. A. **106**, 108 (2002).
[73] Z. Wang, J. Liu, M. Zhang, R.I. Cukier, and Y. Bu, Phys. Rev. Lett. **108**, 207601 (2012).
[74] M.L. Delitsky, and A.L. Lane, J. Geophys. Res. **103**, 31391 (1998).
[75] O. Martinez, Z. Yang, N.J. Demarais, T.P. Snow, and V.M. Bierbaum, Astrophys. J. **720**, 173 (2010).
[76] W.H. Koppenol and J.D. Rush, J. Phys. Chem. **91**, 4429 (1987).
[77] C.E. Klots and R.N. Compton, Bull. Am. Phys. Soc. **23**, 140 (1978).
[78] A. Stamatovic, K. Leiter, W. Ritter, K. Stephan, and T.D. Märk, J. Chem. Phys. **83**, 2942 (1985).
[79] A. Stamatovic, K. Stephan, and T.D. Märk, Int. J. Mass Spec. Ion Proc. **63**, 37 (1985).
[80] E. Leber, S. Barsotti, I. Fabrikant, J.M. Weber, M.W. Ruf, and H. Hotop, Eur. Phys. J. D. **12**, 125 (2000).
[81] S. Barsotti, E. Leber, M.W. Ruf, and H. Hotop, Int. J. Mass Spec. **220**, 313 (2002).
[82] J.P. Gauyacq and A. Herzenberg, Phys. Rev. A. **25**, 2959 (1982).
[83] C.E.H. Dessent, C.G. Bailey, and M.A. Johnson, J. Chem. Phys. **105**, 10416 (1996).
[84] A. Schramm, I. Fabrikant, J.M. Weber, E. Leber, M.W. Ruf, and H. Hotop, J. Phys. B-At. Mol. Opt. Phys. **32**, 2153 (1999).
[85] J.M. Weber, E. Leber, M.W. Ruf, and H. Hotop, Phys. Rev. Lett. **82**, 516 (1999).
[86] C.E.H. Dessent, J. Kim, and M.A. Johnson, Faraday Disc. **115**, 395 (2000).
[87] H. Hotop, M.W. Ruf, M. Allan, and I. Fabrikant, in *Advances in Atomic Molecular, and Optical Physics*, edited by B. Bederson and H. Walther (Elsevier, San Diego, CA, 2003), Vol. 49, pp. 85–216.
[88] H. Hotop, M.W. Ruf, and I. Fabrikant, Phys. Scripta. **T110**, 22 (2004).
[89] I. Fabrikant and H. Hotop, Phys. Rev. Lett. **94**, 063201 (2005).
[90] I. Fabrikant, European Phys. J. D. **35**, 193 (2005).
[91] I. Fabrikant, J. Phys. B - At. Mol. Opt. Phys. **38**, 1745 (2005).
[92] T. Kondow and K. Mitsuke, J. Chem. Phys. **83**, 2612 (1985).
[93] F. Misaizu, K. Mitsuke, T. Kondow, and K. Kuchitsu, J. Chem. Phys. **94**, 243 (1991).
[94] T. Kraft, M.W. Ruf, H. Hotop, and Z. Phys, D. **14**, 179 (1989).
[95] T. Kraft, M.W. Ruf, H. Hotop, and Z. Phys, D. **18**, 403 (1991).
[96] Y. Negishi, T. Nagata, and T. Tsukuda, Chem. Phys. Lett. **364**, 127 (2002).
[97] M.L. Alexander, M.A. Johnson, N.E. Levinger, and W.C. Lineberger, Phys. Rev. Lett. **57**, 976 (1986).
[98] S.H. Fleischman, and K.D. Jordan, J. Phys. Chem. **91**, 1300 (1987).

[99] M. Saeki, T. Tsukuda, and T. Nagata, Chem. Phys. Lett. **340**, 376 (2001).
[100] M. Saeki, T. Tsukuda, and T. Nagata, Chem. Phys. Lett. **348**, 461 (2001).
[101] T. Sommerfeld and T. Posset, J. Chem. Phys. **119**, 7714 (2003).
[102] A.R. Rossi and K.D. Jordan, J. Chem. Phys. **70**, 4422 (1979).
[103] Y. Yoshioka and K.D. Jordan, J. Am. Chem. Soc. **102**, 2621 (1980).
[104] M.J. DeLuca, B. Niu, and M.A. Johnson, J. Chem. Phys. **88**, 5857 (1988).
[105] T. Tsukuda, M.A. Johnson, and T. Nagata, Chem. Phys. Lett. **268**, 429 (1997).
[106] R. Mabbs, E. Surber, and A. Sanov, Chem. Phys. Lett. **381**, 479 (2003).
[107] J.W. Shin, N.I. Hammer, M.A. Johnson, H. Schneider, A. Glöβ, and J.M. Weber, J. Phys. Chem. A. **109**, 3146 (2005).
[108] M. Born, Z. Phys. **1**, 45 (1920).
[109] R. Mabbs, E. Surber, L. Velarde, and A. Sanov, J. Chem. Phys. **120**, 5148 (2004).
[110] M.Z. Kamrath, R.A. Relph, and M.A. Johnson, J. Am. Chem. Soc. **132**, 15508 (2010).
[111] B.J. Knurr and J.M. Weber, J. Phys. Chem. **A 117**, 10771 (2013).
[112] A.M. Ricks, A.D. Brathwaite, and M.A. Duncan, J. Phys. Chem. A. **117**, 11490 (2013).
[113] C.E. Klots, J. Chem. Phys. **83**, 5854 (1985).
[114] J.M. Weber and H. Schneider, J. Chem. Phys. **120**, 10056 (2004).
[115] G. Markovich, R. Giniger, M. Levin, O. Cheshnovsky, and Z. Phys, D. **20**, 69–72 (1991).
[116] D.W. Arnold, S.E. Bradforth, E.H. Kim, and D.M. Neumark, J. Chem. Phys. **97**, 9468 (1992).
[117] D.W. Arnold, S.E. Bradforth, E.H. Kim, and D.M. Neumark, J. Chem. Phys. **102**, 3493 (1995).
[118] D.W. Arnold, S.E. Bradforth, E.H. Kim, and D.M. Neumark, J. Chem. Phys. **102**, 3510 (1995).
[119] A. Osterwalder, M.J. Nee, J. Zhou, and D.M. Neumark, J. Chem. Phys. **121**, 6317 (2004).
[120] Y.X. Zhao, C.C. Arnold, and D.M. Neumark, J. Chem Soc. **89**, 1449 (1993).
[121] M.S. Bowen, M. Becucci, and R.E. Continetti, J. Phys. Chem. A. **109**, 11781 (2005).
[122] F. Mbaiwa, D. Dao, N. Holtgrewe, J. Lasinski, and R. Mabbs, J. Chem. Phys. **136**, 114303 (2012).
[123] A. Sanov, J. Faeder, R. Parson, and W.C. Lineberger, Chem. Phys. Lett. **313**, 812 (1999).
[124] J.M. Weber and H. Schneider, J. Chem. Phys. **122**, 069901 (2005).
[125] A.K. Pathak, ChemPhysChem. **12**, 2641 (2011).
[126] A.K. Pathak, J. Chem. Phys. **136**, 234306 (2012).
[127] K. Hiraoka, T. Shoda, K. Morise, S. Yamabe, E. Kawai, and K. Hirao, J. Chem. Phys. **84**, 2091 (1986).
[128] K. Hiraoka, S. Mizuse, and S. Yamabe, J. Chem. Phys. **87**, 3647 (1987).
[129] D. Ray, N.E. Levinger, J.M. Papanikolas, and W.C. Lineberger, J. Chem. Phys. **91**, 6533 (1989).
[130] J.M. Papanikolas, J.R. Gord, N.E. Levinger, D. Ray, V. Vorsa, and W.C. Lineberger, J. Phys. Chem. **95**, 8028 (1991).
[131] J.M. Papanikolas, V. Vorsa, M.E. Nadal, P.J. Campagnola, J.R. Gord, and W.C. Lineberger, J. Chem. Phys. **97**, 7002 (1992).
[132] J.M. Papanikolas, V. Vorsa, M.E. Nadal, P.J. Campagnola, H.K. Buchenau, and W.C. Lineberger, J. Chem. Phys. **99**, 8733 (1993).
[133] M.E. Nadal, P.D. Kleiber, and W.C. Lineberger, J. Chem. Phys. **105**, 504 (1996).
[134] V. Vorsa, S. Nandi, P.J. Campagnola, M. Larsson, and W.C. Lineberger, J. Chem. Phys. **106**, 1402 (1997).
[135] S. Nandi, A. Sanov, N. Delaney, J. Faeder, R. Parson, and W.C. Lineberger, J. Phys. Chem. A. **102**, 8827 (1998).
[136] A. Sanov, T. Sanford, S. Nandi, and W.C. Lineberger, J. Chem. Phys. **111**, 664 (1999).
[137] T. Sanford, D. Andrews, J. Rathbone, M. Taylor, F. Muntean, M. Thompson, A.B. McCoy, R. Parson, and W. Carl Lineberger, Faraday Disc. **127**, 383 (2004).

[138] T. Sanford, S.Y. Han, M.A. Thompson, R. Parson, and W.C. Lineberger, J. Chem. Phys. **122**, 054307 (2005).
[139] V. Dribinski, J. Barbera, J.P. Martin, A. Svendsen, M.A. Thompson, R. Parson, and W.C. Lineberger, J. Chem. Phys. **125**, 133405 (2006).
[140] M.A. Thompson, J.P. Martin, J.P. Darr, W.C. Lineberger, and R. Parson, J. Chem. Phys. **129**, 224304 (2008).
[141] L. Sheps, E.M. Miller, and W.C. Lineberger, J. Chem. Phys. **131**, 064304 (2009).
[142] L. Sheps, E.M. Miller, S. Horvath, M.A. Thompson, R. Parson, A.B. McCoy, and W.C. Lineberger, Science. **328**, 220 (2010).
[143] L. Sheps, E.M. Miller, S. Horvath, M.A. Thompson, R. Parson, A.B. McCoy, and W.C. Lineberger, J. Chem. Phys. **134**, 184311 (2011).
[144] P.E. Maslen, J.M. Papanikolas, J. Faeder, R. Parson, and S.V. ONeil, J. Chem. Phys. **101**, 5731 (1994).
[145] N. Delaney, J. Faeder, P.E. Maslen, and R. Parson, J. Phys. Chem. A. **101**, 8147 (1997).
[146] J. Faeder, N. Delaney, P.E. Maslen, and R. Parson, Chem. Phys. **239**, 525 (1998).
[147] N. Delaney, J. Faeder, and R. Parson, J. Chem. Phys. **111**, 452 (1999).
[148] N. Delaney, J. Faeder, and R. Parson, J. Chem. Phys. **111**, 651 (1999).
[149] R. Parson, J. Faeder, and N. Delaney, J. Phys. Chem. A. **104**, 9653 (2000).
[150] J.R. Faeder and R. Parson, J. Phys. Chem. A. **114**, 1347 (2010).
[151] A.S. Case, A.B. McCoy, and W.C. Lineberger, J. Phys. Chem. A. **117**, 13310 (2013).
[152] J.P. Martin, A.S. Case, Q. Gu, J.P. Darr, A.B. McCoy, and W.C. Lineberger, J. Chem. Phys. **139**, 064315 (2013).
[153] R. Wester, A.V. Davis, A.E. Bragg, and D.M. Neumark, Phys. Rev. A. **65**, 051201 (2002).
[154] M.T. Zanni, B.J. Greenblatt, and D.M. Neumark, J. Chem. Phys. **109**, 9648 (1998).
[155] A.V. Davis, M.T. Zanni, C. Frischkorn, M. Elhanine, D.M. Neumark, and J. El, Spectrosc. Rel. Phenom. **112**, 221 (2000).
[156] R. Parson and J. Faeder, Science. **276**, 1660 (1997).
[157] L.A. Posey, M.J. DeLuca, P.J. Campagnola, and M.A. Johnson, J. Phys. Chem. **93**, 1178 (1989).
[158] S.T. Arnold, R.A. Morris, A.A. Viggiano, and M.A. Johnson, J. Phys. Chem. **100**, 2900 (1996).
[159] O.P. Balaj, C.K. Siu, I. Balteanu, M.K. Beyer, and V.E. Bondybey, Chem. Eur. J. **10**, 4822 (2004).
[160] C.E. Klots, J. Chem. Phys. **71**, 4172 (1979).
[161] X. Yang and A.W. Castleman, J. Am. Chem. Soc. **113**, 6766 (1991).
[162] J.M. Weber, J.A. Kelley, S.B. Nielsen, P. Ayotte, and M.A. Johnson, Science. **287**, 2461 (2000).
[163] R.F. Höckendorf, C.K. Siu, C. van der Linde, O.P. Balaj, and M.K. Beyer, Angew. Chem. Int. Ed. **49**, 8257 (2010).
[164] R.F. Höckendorf, Q. Hao, Z. Sun, B.S. Fox-Beyer, Y. Cao, O.P. Balaj, V.E. Bondybey, C.K. Siu, and M.K. Beyer, J. Phys. Chem. A. **116**, 3824 (2012).
[165] R.F. Höckendorf, K. Fischmann, Q. Hao, C. van der Linde, O.P. Balaj, C.K. Siu, and M.K. Beyer, Int. J. Mass Spec. **354**–**355**, 175 (2013).
[166] A. Akhgarnusch, R.F. Höckendorf, Q. Hao, K.P. Jäger, C.K. Siu, and M.K. Beyer, Angew. Chem. Int. Ed. **52**, 9327 (2013).
[167] T. Tsukuda and T. Nagata, J. Phys. Chem. A. **107**, 8476 (2003).
[168] A. Akhgarnusch and M.K. Beyer, Int. J. Mass Spec. **365**–**366**, 295 (2014).
[169] A. Muraoka, Y. Inokuchi, N. Nishi, and T. Nagata, J. Chem. Phys. **122**, 094303 (2005).
[170] W.H. Robertson, E.A. Price, J.M. Weber, J.W. Shin, G.H. Weddle, and M.A. Johnson, J. Phys. Chem. A. **107**, 6527 (2003).
[171] P. Ayotte, G.H. Weddle, J. Kim, and M.A. Johnson, Chem. Phys. **239**, 485 (1998).
[172] E. Surber, R. Mabbs, T. Habteyes, and A. Sanov, J. Phys. Chem. A. **109**, 4452 (2005).
[173] L. Velarde, T. Habteyes, and A. Sanov, J. Chem. Phys. **125**, 114303 (2006).

[174] T. Habteyes, L. Velarde, and A. Sanov, Chem. Phys. Lett. **424**, 268 (2006).
[175] T. Habteyes, L. Velarde, and A. Sanov, J. Chem. Phys. **126**, 154301 (2007).
[176] K.J. Breen, A.F. DeBlase, T.L. Guasco, V.K. Voora, K.D. Jordan, T. Nagata, and M.A. Johnson, J. Phys. Chem. A. **116**, 903 (2012).
[177] A. Muraoka, Y. Inokuchi, N.I. Hammer, J.W. Shin, M.A. Johnson, and T. Nagata, J. Phys. Chem. A. **113**, 8942 (2009).
[178] T. Tsukuda, M. Saeki, R. Kimura, and T. Nagata, J. Chem. Phys. **110**, 7846 (1999).
[179] M. Saeki, T. Tsukuda, S. Iwata, and T. Nagata, J. Chem. Phys. **111**, 6333 (1999).
[180] K. Hiraoka and S. Yamabe, J. Chem. Phys. **97**, 643 (1992).
[181] H. Schneider, A.D. Boese, and J.M. Weber, J. Chem. Phys. **123**, 074316 (2005).
[182] M.E. Jacox and W.E. Thompson, J. Phys. Chem. **95**, 2781 (1991).
[183] K. Sudoh, Y. Matsuyama, A. Muraoka, R. Nakanishi, and T. Nagata, Chem. Phys. Lett. **433**, 10 (2006).
[184] S.Y. Han, I. Chu, J.H. Kim, J.K. Song, and S.K. Kim, J. Chem. Phys. **113**, 596 (2000).
[185] S.H. Lee, N. Kim, D.G. Ha, and S.K. Kim, J. Am. Chem. Soc. **130**, 16241 (2008).
[186] N. Kim, Bull. Korean Chem. Soc. **34**, 2247 (2013).
[187] T. Tsukuda, M. Saeki, and T. Nagata, Chem. Phys. Lett. **251**, 309 (1996).
[188] T. Tsukuda, M. Saeki, S. Iwata, and T. Nagata, J. Phys. Chem. A. **101**, 5103 (1997).
[189] M. Haruta and M. Daté, Appl. Catal. A. **222**, 427 (2001).
[190] A. Sanchez, S. Abbet, U. Heiz, W.D. Schneider, H. Häkkinen, R.N. Barnett, and U. Landman, J. Phys. Chem. A. **103**, 9573 (1999).
[191] U. Heiz and W.D. Schneider, J. Phys. D - Appl. Phys. **33**, R85 (2000).
[192] J. Hagen, L.D. Socaciu, M. Elijazyfer, U. Heiz, T.M. Bernhardt, and L. Wöste, Phys. Chem. Chem. Phys. **4**, 1707 (2002).
[193] L.D. Socaciu, J. Hagen, T.M. Bernhardt, L. Wöste, U. Heiz, H. Häkkinen, and U. Landman, J. Am. Chem. Soc. **125**, 10437 (2003).
[194] M.L. Kimble, A.W. Castleman, R. Mitrić, C. Bürgel, and V. Bonačić-Koutecký, J. Am. Chem. Soc. **126**, 2526 (2004).
[195] K. Tanaka and D. Ooyama, Coordin. Chem. Rev. **226**, 211 (2002).
[196] Z.F. Chen, C.C. Chen, D.R. Weinberg, P. Kang, J.J. Concepcion, D.P. Harrison, M.S. Brookhart, and T.J. Meyer, Chem. Commun. **47**, 12607 (2011).
[197] A. Cho, Science. **299**, 1684 (2003).
[198] B.J. Knurr, and J.M. Weber, J. Am. Chem. Soc. **134**, 18804 (2012).
[199] B.J. Knurr and J.M. Weber, J. Phys. Chem. A. (submitted).
[200] A.D. Boese, H. Schneider, A.N. Glöß, and J.M. Weber, J. Chem. Phys. **122**, 154301 (2005).
[201] B.J. Knurr and J.M. Weber, J. Phys. Chem. A. **118**, 4056 (2014).
[202] B.J. Knurr and J.M. Weber, J. Phys. Chem. A. **118**, 8753–8757 (2014).
[203] D.H. Gibson, Chem. Rev. **96**, 2063 (1996).
[204] G.E. Johnson, E.C. Tyo, and A. W. Castleman. J. Phys. Chem. A. **112**, 4732 (2008).
[205] P.A. Hintz and K.M. Ervin, J. Chem. Phys. **103**, 7897 (1995).
[206] E. Hossain, D.W. Rothgeb, and C.C. Jarrold, J. Chem. Phys. **133**, 024305 (2010).
[207] D.W. Rothgeb, E. Hossain, J.E. Mann, and C.C. Jarrold, J. Chem. Phys. **132**, 064302 (2010).
[208] J.E. Mann, N.J. Mayhall, and C.C. Jarrold, Chem. Phys. Lett. **525**–**526**, 1 (2012).
[209] M. Brümmer, C. Kaposta, G. Santambrogio, and K.R. Asmis, J. Chem. Phys. **119**, 12700 (2003).
[210] X.B. Wang, H.K. Woo, and L.S. Wang, J. Chem. Phys. **123**, 051106 (2005).
[211] X.B. Wang and L.S. Wang, Rev. Sci. Instrum. **79**, 073108 (2008).
[212] A.B. Wolk, C.M. Leavitt, E. Garand, and M.A. Johnson, Accounts Chem. Res. **47**, 202 (2014).